

Contents lists available at ScienceDirect

Organic Geochemistry

journal homepage: www.elsevier.com/locate/orggeochem





Molecular and optical characterization reveals the preservation and sulfurization of chemically diverse porewater dissolved organic matter in oligohaline and brackish Chesapeake Bay sediments

Leanne C. Powers ^{a,*,1}, Laura L. Lapham ^a, Sairah Y. Malkin ^b, Andrew Heyes ^a, Philippe Schmitt-Kopplin ^{a,c,d}, Michael Gonsior ^{a,*}

- ^a University of Maryland Center for Environmental Science, Chesapeake Biological Laboratory, Solomons, MD, USA
- ^b University of Maryland Center for Environmental Science, Horn Point Laboratory, Cambridge, MD, USA
- c Helmholtz Zentrum Muenchen German Research Center for Environmental Health, Research Unit Analytical BioGeoChemistry, D-85764 Neuherberg, Germany
- ^d Technische Universität München, Chair of Analytical Food Chemistry, D-85354 Freising-12 Weihenstephan, Germany

ARTICLE INFO

Associate Editor-Elizabeth Minor

Keywords:
Porewater DOM
Sulfurization
FT-ICR MS
Chesapeake Bay
Algal DOM
Brackish
Oligohaline
EEM

ABSTRACT

In this study, we conducted a detailed analysis of porewater downcore chemical properties and porewater dissolved organic matter (PDOM) composition using elemental C, N and S analysis, fluorescence spectroscopy, and ultrahigh resolution mass spectrometry (FT-ICR MS) at two contrasting sites in Chesapeake Bay. The sites, situated in the oligohaline upper bay and in the seasonally hypoxic mesohaline mid bay, receive fundamentally different detrital inputs predominantly from allochthonous and autochthonous sources, respectively. Unsurprisingly, we observed greater molecular oxygenation and degree of aromaticity in downcore PDOM profiles from the upper bay. At the mid bay station, PDOM composition was more indicative of non-aromatic algalderived material. Unexpectedly, this autochthonous PDOM had lower C:S ratios. Hence, algal-derived organic matter appeared to be readily sulfurized, which was confirmed by quantification of dissolved organic sulfur as well as by qualitative interpretation of FT-ICR MS data. This finding suggests addition reactions of hydrogen sulfide to double bonds in unsaturated, but non-aromatic, organic molecules in autochthonous PDOM. Intriguingly, we also observed increases in humic-like fluorescence and dissolved organic carbon (DOC) concentrations in downcore PDOM profiles from both sites. Given the differences in molecular composition between sites, these results show that humic-like fluorescence can arise from different sources and biogeochemical processes. In the upper bay, we infer that these fluorescence signals reflect solubilization of terrestrially derived organic matter with a high aromatic and polyphenolic composition. By contrast, in the mid bay, these fluorescence peaks correlated negatively with hydrogen sulfide and are more likely linked to bacterial sulfate reduction.

1. Introduction

Estuaries and coastal zones play a disproportionately large role in marine dissolved organic matter (DOM) cycling (Bauer et al., 2013). However, given the complexities and dynamics of shallow aquatic systems, and the complex and largely uncharacterized nature of DOM, understanding the sources, sinks, and transformations of estuarine and coastal DOM is extremely challenging (Osterholz et al., 2016; Powers et al., 2018). Significant organic matter mineralization and transformation occurs in estuarine sediments, which play a central role in

seasonal and longer-term regulation of nutrient and DOM cycling. Early diagenesis of organic matter in sediments typically yields a predictable downcore accumulation of refractory DOM, often identified as humic-like fluorescent DOM (FDOM) (Burdige et al., 2004; Clark et al., 2014; He et al., 2016). This porewater DOM (PDOM) may be further transformed, buried, or may diffuse or resuspend into the water column where it may be a quantitatively significant source to the DOM budget (Burdige and Homstead, 1994). Thus, a better understanding of the formation pathways and fate of porewater organic carbon is important for constraining estuarine carbon cycle models, as well as to better

^{*} Corresponding authors.

E-mail addresses: lcpowers@esf.edu (L.C. Powers), gonsior@umces.edu (M. Gonsior).

¹ Present address: State University of New York, College of Environmental Science and Forestry, Department of Chemistry, Syracuse, NY, USA.

understand sediment diagenesis and sequestration of carbon.

DOM that absorbs energy at short wavelengths (ultraviolet (UV)visible light) and emits a portion of that energy as fluorescence at much longer wavelengths traditionally has been described as having 'humiclike' optical properties. In near-shore environments receiving large quantities of riverine inputs, the degradation products of terrestrially derived lignin polyphenols are positively correlated with the intensity of these humic-like optical properties (Hernes et al., 2008; Spencer et al., 2008; Boyle et al., 2009). However, other water column studies have proposed different origins of humic-like optical properties, such as microbial transformation of particulate (Nelson et al., 1998, 2007; Nelson and Siegel, 2013) or dissolved autochthonous source material (Yamashita et al., 2007; Yamashita and Tanoue, 2008), which includes possible direct links to specific organisms such as picocyanobacteria (Zhao et al., 2017). For example, humic-like fluorescence was ubiquitous in Antarctic lakes and streams (Kida et al., 2019), and present in glacial meltwater (Kida et al., 2021), despite having non-aromatic DOM reflective of its microbial source. In the estuarine sediments of Chesapeake Bay, it was previously suggested that humic-like FDOM in porewater could result from both terrestrial refractory organic matter and/or in situ diagenetic alteration of DOM or FDOM (Burdige et al., 2004). Higher relative humic-like fluorescence was observed in anoxic mid bay sediments than in oxic/anoxic lower bay sediments, suggesting that humic-like FDOM is preferentially preserved under anoxic conditions (Burdige, 2001).

The early diagenesis of PDOM is characterized by a cascade of biogeochemical activities associated with the availability of terminal electron acceptors (oxygen, nitrate, iron (Fe), manganese (Mn), sulfate) at different sediment depths. This process includes the formation of methane after the depletion of sulfate; which utilizes the electron acceptors within PDOM itself. The production of highly fluorescent PDOM in sediment porewater has thus far only been associated with sulfate reduction and, to a lesser extent, fermentation (Chen et al., 2016; Luek et al., 2017). This fluorescent PDOM also has similar fluorescence properties to humic-like FDOM (Chen et al., 2016; Luek et al., 2017). Therefore, it is unclear whether the source of humic-like FDOM in sediments is a result of its refractory nature and similarity to terrigenous material or its recent production by sulfate reducing bacteria.

While the mechanistic link between sulfate reduction and FDOM production is not entirely clear, sulfate reduction produces hydrogen sulfide (H2S), which in turn reacts with DOM by a suite of diverse sulfurization reactions (Pohlabeln et al., 2017). In the sulfate reduction zone, PDOM can react directly with H₂S or polysulfides, or undergo microbial sulfurization to form S-containing organic compounds (De Graaf et al., 1992; Schouten et al., 1993, 1994). While early work suggested that sulfurization mainly occurs through a Michael addition of sulfur to activated double bonds (Vairavamurthy and Mopper, 1987), recent work has demonstrated that sulfur incorporation into DOM is relatively unselective (Pohlabeln et al., 2017), quantitatively important and fast (Heitmann and Blodau, 2006). After other terminal electron acceptors become depleted in sediments (e.g., O2, NO3, Mn, Fe), sulfate reduction is constrained by the supply rate of sulfate and labile organic carbon, and may be further kinetically controlled by temperature. Given the large supply of sulfate in estuaries compared to many freshwater systems, estuaries are suspected to be sites where extensive sulfate reduction and DOM sulfurization can occur (Francois, 1987; Ferdelman et al., 1991; Brüchert, 1998).

The production of dissolved organic sulfur (DOS) in sediment porewater may mark the first step towards organic matter sequestration. This is supported by studies investigating sediment carbon and sulfur (Francois, 1987; Peterson and Howarth, 1987; Ferdelman et al., 1991; Burdige and Homstead, 1994; Brüchert, 1998; Zimmerman and Canuel, 2001) as well as optical properties (e.g., fluorescence) of porewaters (Burdige et al., 2004; Clark et al., 2014; He et al., 2016). Previous studies that have described the PDOM composition in greater detail have also shown a diverse suite of organic sulfur signatures using high resolution mass spectrometry (HRMS) (Schmidt et al., 2009, 2011). Even under

conditions of low salinity (i.e., salinity < 7), if there is a sufficiently high organic matter loading, a majority of authigenic organic sulfur may escape re-oxidation in surface sediments to become buried (Thang et al., 2013). Thus, the sulfurization of DOM may also be linked to the production of refractory DOM and potentially humic-like FDOM.

Unfortunately, the observation of broad humic-like FDOM alone is insufficient in describing associated chemical signatures. Furthermore, discussions of the concomitant changes in humic-like FDOM and the molecular composition of PDOM with sediment depth is rare (Derrien et al., 2018). A few studies have performed detailed molecular-level characterization of porewater DOM using HRMS (i.e., Fourier transform ion cyclotron resonance mass spectrometry, FT-ICR MS) in marine (Schmidt et al., 2009, 2011, 2017; Seidel et al., 2014; Rossel et al., 2016; Abdulla et al., 2020) and freshwater sediments (D'Andrilli et al., 2010; Herzsprung et al., 2017; Poulin et al., 2017; Valle et al., 2018). This work has revealed a large diversity of DOS molecules in marine sediments (Schmidt et al., 2009; Seidel et al., 2014; Abdulla et al., 2020). Recent work used FT-ICR MS to investigate possible mechanisms of DOS formation in the anoxic sediments of the Santa Barbara basin (Abdulla et al., 2020). Their study suggested that addition reactions of sulfide and polysulfide to molecular formulas associated with carboxyl-rich alicyclic molecules (CRAMs) were the major pathways for DOS formation (Abdulla et al., 2020), although reaction pathways could not be confirmed.

To better understand potential mechanisms involved in rendering porewater DOM refractory and any potential relationships to humic-like FDOM, detailed evaluations of the molecular composition of porewater DOM are required. Therefore, our primary goal was to provide new insights on the molecular complexity of porewater DOM associated with PDOM preservation and sulfurization at contrasting sites from the mainstem of Chesapeake Bay. We selected an upper bay oligohaline station that is located 30 km south of the Susquehanna River mouth where sediment transport from the river plume routinely extend (Zheng et al., 2015). Sulfate reduction rates are very low in the upper bay associated with low sulfate concentrations and inputs of DOM primarily of terrestrial origin (Marvin-DiPasquale et al., 2003). For contrast, we also selected a mesohaline mid bay station where bottom water sulfate concentration is high, and where sediments contain a high proportion of organic matter derived from autochthonous production and support high rates of sulfate reduction (Marvin-DiPasquale et al., 2003). Previous foundational research on organic matter composition of Chesapeake Bay sediments reported down core increases in humic-like FDOM (Burdige et al., 2004), and additionally reported site-to-site differences in PDOM composition between these specific sites (Burdige, 2001). Therefore, we aimed to compare humic-like fluorescence signals in sediments from both stations to assess if fluorophores derived from putatively very different sources have convergent 3D fluorescence signatures. In particular, we relied on 3D fluorescence and absorbance spectroscopy, and ultrahigh resolution FT-ICR MS interfaced with negative mode electrospray ionization (ESI). Finally, we conducted complimentary quantitative analyses of down core chemical properties (i.e., chloride, sulfate, hydrogen sulfide, dissolved organic carbon (DOC) and sulfur (DOS) as well as methane) to give a broad geochemical context for our data.

2. Methods

2.1. Sample collection and non-PDOM analysis

The upper bay station (herein "UB"), representing the main channel in the oligohaline zone, lies approximately 30 km south of the Susquehanna River mouth at $\sim \! 13$ m water depth, and bottom waters are generally well-oxygenated year-round, supporting infaunal communities dominated by polychaetes and bivalves. The mid bay station (herein, "MB"), located $\sim \! 95$ km downstream of the Susquehanna River, was chosen to represent the main channel in the mesohaline zone (mean

salinity of ~19 ppt). MB bottom waters experience severe summer hypoxia between May and September, and consequently there is negligible bioturbation activity from benthos (Sturdivant et al., 2014). Additional information on these study sites and Chesapeake Bay is provided in the Supplementary Materials. Sediment cores were collected on September 6, 2017 aboard the R/V Rachel Carson (Maryland, USA) using a gravity corer (Model GC-150; Mooring Systems, Inc; Cataumet, MA, USA), with core liners made of cellulose acetate butyrate (inner diameter \sim 6.7 cm). Two cores were collected at each site: one for methane analysis and the other for all other chemical analyses. Once retrieved, sediment cores were inspected for an undisturbed sedimentwater interface and high-quality cores were capped. Methane sampling was performed using core liners with pre-drilled holes at 2.0 cm increments. Within minutes of core retrieval, 3 mL cut-off syringes were used to subsample from the pre-drilled holes in the core liners. Sediment was transferred immediately to 40 mL serum vials, preserved with 6 mL of 2.5% NaOH, crimped sealed, shaken vigorously, and stored upsidedown onboard the ship. These samples were then stored at -20 °C until further analysis. Methane concentrations were analyzed by gas chromatography-flame ionization detection (SR 8610C). At UB, porewater was additionally sampled from 1 to 2 cm core sections for a highresolution profile of additional analyses. These analyses included NH₄ and Fe(II) concentrations, which were analyzed colorimetrically by phenol-hypochlorite (Helder and De Vries, 1979) and ferrozine (Viollier et al., 2000), respectively.

Remaining sediment cores collected from both sites were returned to the laboratory and sectioned within 12 h of collection. Sediment cores were sectioned by extruding sediment from the bottom of the core liner (inner diameter ~6.7 cm) using a plunger into 5 or 10 cm open cellulose acetate butyrate cylinders with the same inner diameter as the core liner. Sections were sliced with a Plexiglas sheet, providing 5-10 cm whole round sections from various depths along the core (sectioning occurred at 5, 10, 15, 25, 35, 45, 55, 65 cm at UB and at 10, 20, 30, 40, 50, 60, and 70 cm at MB). Sediment from each section were then packed into 50 mL polypropylene centrifuge tubes (VWR Scientific) with no head space and sealed, taking care to avoid sediment that had been in contact with the walls of the core liners. Contact with the atmosphere was unavoidable using this approach and the oxidation of DOM, as well as ferrous iron and sulfide, cannot be completely ruled out. However, to ensure that DOM oxidation was minimized, sediment porewater was extracted immediately after sectioning to minimize oxygen exposure and porewater DOM oxidation.

Porewater was extracted by centrifugation (Sorvall® RT 6000D centrifuge; 30 min at 20 °C, 3000 rpm, relative centrifugal forced = 1877 g). It should be noted that centrifugation can elevate porewater DOC concentrations and DOM optical properties compared to other porewater extraction techniques (i.e. Rhizon sampling) (Chen et al., 2015). Nevertheless, our results are comparable with previous work that has used centrifugation (Burdige and Zheng, 1998). Moreover, while the presence of macrofauna may also cause variability in DOC concentrations determined in porewater collected by centrifugation (Martin and McCorkle, 1993), we only observed a few bivalves in the surface sediments at UB during our sampling. After centrifugation, tubes were placed under N2 atmosphere in a glove bag (Coy Laboratory Products). Splits were taken for sulfate and chloride analyses (0.5 mL acidified using 50 µL concentrated H₃PO₄, MQ200, EMD Millipore) using an ion chromatography system (Dionex ICS-1000). The remaining porewater was filtered through 0.2 µm syringe filters (Whatman 25 mm GD/X cellulose acetate). All filters were previously rinsed with at least 60 mL ultrapure water (Barnstead 18 $M\Omega$ Milli-Q water) and flushed with at least 3 mL of sample before collecting the filtrate. An aliquot was prepared for analysis of hydrogen sulfide (H2S/HS-), which was determined for filtered porewater samples using an Orion silver/sulfide electrode model 94-16 with an Orion double junction reference electrode model 90-20. Samples were diluted 1:1 with antioxidant buffer under N₂ to preserve the sulfide ion. Antioxidant buffer contained 2.0 M

NaOH (ACS grade, J.T. Baker), 0.2 M ethylenediaminetetraacetic acid disodium salt dihydrate (ACS grade, J.T. Baker), and 0.2 M L-ascorbic acid (ACS grade, VWR Scientific) and was prepared in deoxygenated pure water (boiled under N_2). A sulfide stock solution was prepared by dissolving 10 g $Na_2S\cdot 9H_2O$ (Sigma-Aldrich) in 5 mL deoxygenated water and stored under N_2 . Sulfide standards ranging from 100 nM to 10 mM were prepared by diluting the stock solution with antioxidant buffer, which is a sufficient range for the samples analyzed in this work. However, it should be noted that this method does not account for total dissolved sulfides or polysulfides (Cline, 1969; Luther et al., 1985), so "sulfide" concentrations may be underestimated in this study.

2.2. Solid-phase extraction of PDOM

PDOM was extracted using an established solid phase extraction (SPE) procedure and 200 mg Agilent Bond Elut PPL cartridges (Dittmar et al., 2008), with minor modifications. Briefly, filtered porewater was acidified to pH 2 with concentrated HCl (Sigma Aldrich 32%, pura) and pipetted onto activated PPL cartridges in an anaerobic glove bag under N₂ atmosphere. Final extraction volumes ranged from 9 to 39 mL. After extraction, the PPL cartridges were rinsed with 0.1% formic acid (LC-MS. Sigma Aldrich), dried at room temperature, and eluted with 4 mL pure methanol (LC-MS, Sigma Aldrich). Aliquots of the methanolic extracts (0.2-0.6 mL) were dried in the anaerobic glove bag under N₂, then re-dissolved in pure water to a final dilution factor of 15-40. These extracts (herein, "SPE-PDOM") were subsequently analyzed for optical properties and for carbon, nitrogen, and sulfur concentrations, described below. SPE blanks were prepared by passing 1 L of pH 2 ultrapure water through a PPL cartridge and processed as described above. Remaining aliquots of the methanolic extracts were stored at −20 °C until analysis by FT-ICR MS, as described below.

2.3. Total dissolved nitrogen (TDN), dissolved organic carbon (DOC), dissolved organic nitrogen (DON) and dissolved organic sulfur (DOS)

Filtered porewater samples were diluted 1:10 with ultrapure water and SPE-PDOM samples were diluted as described above. All samples were acidified to pH 2 and DOC and TDN were measured by high temperature combustion (Shimadzu TOC-V_{CPH}). Potassium hydrogen phthalate and potassium nitrate (extra pure, Acros Organics) were used as DOC and TDN standards, respectively. SPE-PDOM blanks and samples washed with diluted HCl (pH 2), instead of 0.1% formic acid, were checked for DOC contamination. After correcting for added DOC, SPE-DOC concentrations were adjusted for extraction volume and dilution and DOC extraction efficiencies were determined as the percentage of DOC contained in the SPE-PDOM sample when compared to the DOC in the porewater sample. Assuming SPE-PDOM does not contain inorganic nitrogen, TDN measurements of SPE-PDOM are reported as SPEdissolved organic nitrogen (DON). Because we did not measure inorganic nitrogen species separately, we cannot determine the DON extraction efficiency for our samples. However, all SPE-DON values reported here are also corrected for dilution and extraction volume.

DOS was determined for SPE-PDOM samples using a Triple Quadrupole inductively coupled plasma-mass spectrometer (ICP-MS-MS, Agilent 8900 ICP-QQQ) equipped with a collision/reaction cell following slight modifications to established methods (Ksionzek et al., 2016; Ossola et al., 2019). To improve sulfur detection and minimize interferences, oxygen gas was reacted with sulfur to form $^{32}S^{16}O$ in the collision cell. Sulfur was then determined using m/z 32 (MS1) and m/z 48 (MS2) with an integration time of 0.5 ms, 1 point per peak, 3 replicates and 50 sweeps per replicate. The ICP was tuned weekly using a multi-element tuning solution containing Li, Co, Y, Tl, and Ce (Agilent) diluted to 1 μ g L $^{-1}$ with pure water. SPE-PDOM samples were further diluted to a final dilution factor of 1000 for ICP-MS analysis. ^{59}CO (Agilent) was used as an internal standard in all samples, blanks, and standards at a final concentration of 0.5 μ g L $^{-1}$. Standard curves were

prepared from 0 to 50 ppb using dilutions of a 10 ppm multi-element calibration mix (Agilent) and were in agreement to those made using dilutions of $\rm Na_2S_2O_3$ (>99.99% trace metal basis, Sigma-Aldrich). A sulfur containing organic compound (3-chloro-4-(sulfonyl)thiophene-2 carboxylic acid, Sigma-Aldrich) was also analyzed to assess the accuracy of sulfur determination and was within 5% of expected concentration. Like SPE-DON, extraction efficiencies could not be determined for SPE-DOS but were also corrected for extraction volume and dilution.

C:N, C:S, and N:S ratios were determined for all SPE-PDOM samples using corrected concentrations, as described above. However, before calculating these ratios, SPE-DOC, SPE-DON, and SPE-DOS were converted to molar concentrations using 12.01 g/mol (DOC), 14.007 g/mol (DON), and 32.066 g/mol (DOS), respectively.

2.4. Determination of optical properties of PDOM and SPE-PDOM.

Chromophoric DOM (CDOM) absorbance spectra (A(λ)) and excitation emission matrix (EEM) fluorescence spectra were measured using a spectrofluorometer (Horiba Aqualog System) for filtered porewater samples and SPE-PDOM samples. SPE-PDOM samples were prepared as described previously (Section 2.2). Because absorbance at low wavelengths was outside of the linear range of the instrument for several porewater samples (i.e. $A(\lambda) > 2$), all porewater samples were diluted 1:10 with 18 M Ω Milli-Q water prior to analysis. Dilution may change chemical properties but mathematical inner filter corrections may not rectify EEM spectra of undiluted samples, especially when absorbance values are not reliable (Larsson et al., 2007; Murphy et al., 2010).

Excitation or $A(\lambda)$ spectra were collected at 3 nm intervals between 230 and 600 nm and emission spectra were collected at fixed 3.26 nm intervals between 235 and 600 nm. Ultrapure water served as the absorbance and fluorescence blank and the water Raman peak was measured daily to monitor and correct for possible instrument drift.

EEM spectra were corrected for Raleigh scattering following a method established previously (Zepp et al., 2004) and for inner filter effects using the Aqualog software. EEM spectra were normalized to the emission area (excitation = 347 nm) of a 1 ppm Starna quinine sulfate standard in 0.1 M $\rm HClO_4$. Thus, fluorescence intensities reported here are expressed in quinine sulfate units (QSU, ppm). Fluorescence conventional humic-like A- and C-peak intensities were determined by finding fluorescence maxima ($\rm F_{max}$) within pre-defined excitation (ex) and emission (em) peak boundaries (Coble, 1996).

$$A - peak = F_{max}(ex < 260 \text{ nm}; em 400 \text{ to } 460 \text{ nm})$$
 (1)

$$C - peak = F_{max}(ex 320 \text{ to } 360 \text{ nm}; em 420 \text{ to } 460 \text{ nm})$$
 (2)

Post analysis, EEM spectra and calculated parameters (Equations (1) and (2)) were corrected for dilution, and in the case of SPE-PDOM samples, scaled for extraction and elution volume.

2.5. SPE-PDOM characterization using FT-ICR MS

All methanolic extracts were diluted 1:20 with pure methanol prior to direct infusion into the negative mode electrospray interface of a Bruker Solarix 12 Tesla FT-ICR MS at a flow rate of 2 μ L min⁻¹. The FT-ICR MS was pre-calibrated using known clusters of arginine. Five hundred scans were collected at 4 megaword data points and spectra were averaged over an m/z range of 140–1000. Spectra were post-calibrated using known DOM m/z ions ranging from m/z 213–711 and peak lists were exported using a signal-to-noise ratio cutoff \geq 10 using the Bruker DataAnalysis 4.0 software (Timko et al., 2015b). Exported masses were aligned within a m/z window of 0.5 ppm using proprietary Matrix Generator software (Lucio, 2009) and molecular formulas were assigned using a mass difference approach and proprietary software, NetCalc (Tziotis et al., 2011). Unambiguous exact molecular formulas were computed based on elemental combinations of $^{12}C_{1-\infty}$, $^{14}H_{1-\infty}$, $^{16}O_{1-\infty}$, $^{14}N_{0-5}$, $^{32}S_{0-3}$, and isotopologues with a mass error of < 0.2 ppm.

Formula assignments were only considered valid if they were chemically possible and met the criteria outlined in previous studies (Koch et al., 2007; Herzsprung et al., 2014).

Throughout this study, molecular ion relative abundances and intensity-weighted average (wt) characteristics were used to compare formula assignments between samples. van Krevelen or elemental diagrams (van Krevelen, 1950) were used to visualize FT-ICR MS data by plotting H/C ratios vs O/C ratios for all assigned molecular formulas, thereby revealing bulk properties like the degree of saturation and oxygenation (van Krevelen, 1950). Modified Kendrick diagrams, or plots of the Kendrick mass defect (KMD) (Kendrick, 1963) normalized to the z-score (z*) vs exact mass (m/z) (Stenson et al., 2003; Shakeri Yekta et al., 2012), were used to visualize homologous series of formulas based on CH₂ spacing in the horizontal direction, -CH₄/+O spacing in the vertical direction, and H₂ spacing in the diagonal direction (Stenson et al., 2003; Shakeri Yekta et al., 2012; Gonsior et al., 2019). A few additional parameters were calculated to gain additional information based on assigned molecular formulas. Namely, double bond equivalents (DBE), or the number of unsaturations plus rings in a molecule, were determined for assigned molecular formulas according to the equation below (Koch and Dittmar, 2006)

$$DBE = 1 + \sum N_{x}(V_{x} - 2)/2$$
 (3)

where N_x is the number of atoms of element x and V_x is the valence of element x. The average carbon oxidation state (COS) was also computed for all formula assignments. COS was approximated by:

$$COS = (2(O+S) + 3N - H)/C$$
 (4)

where formulas with COS values less than or equal to 0 indicates reduced molecules and formulas with COS values greater than zero indicates oxidized molecules (Kroll et al., 2011).

To explore possible sulfurization reactions, assigned molecular formulas were used to construct mass difference networks using NetCalc where precisely measured ion masses with assigned molecular formulas (nodes) were connected by mass differences (edges) (Tziotis et al., 2011; Gonsior et al., 2019). For example, the H₂S Michael addition reaction (+H₂S = 33.987721 Da) was tested between possible CHO precursors and CHOS products and between CHNO precursors and CHNOS products. Additional possible reactions that would incorporate sulfur into the DOM pool were tested. The reactions that could explain a similar number of CHOS/CHNOS formulas as the H₂S addition reaction were +H₂S/-H₂ = 31.972071 Da, +H₂S/-2H₂ = 29.956421 Da, +H₂S/-H₂O = 15.977156 Da, and +H₂S/+H₂O/-2H₂ = 47.966986 Da.

To statistically assess similarities and differences in DOM composition between sites and with depth, we also performed a two-dimensional hierarchical cluster analysis (HCA) of all m/z ions with assigned molecular formulas (Powers et al., 2018; Shakeri Yekta et al., 2012). The m/ z ion intensities were log-transformed and centered using the median, then similarity scores were computed using Pearson's correlations (Eisen et al., 1999). Cluster 3.0 software was used to run the HCA using average linkages of the similarity scores (Eisen et al., 1999). A dendrogram was generated using Java Treeview and used to visualize the results of the HCA and to determine major clusters within the dataset (Saldanha, 2004). In the dendrogram, two indicative clusters were identified for each site and had Pearson's correlations of 0.5-1.0 and high log-transformed ion intensities for the majority of the sediment core. The results of this analysis can further describe which m/z ions, and therefore which molecular formulas, are associated with either the UB site or the MB site.

3. Results and discussion

3.1. Chemical properties of sediment porewater in the upper and mid bay

At UB, the DOC, TDN, and NH₄ concentration profiles generally

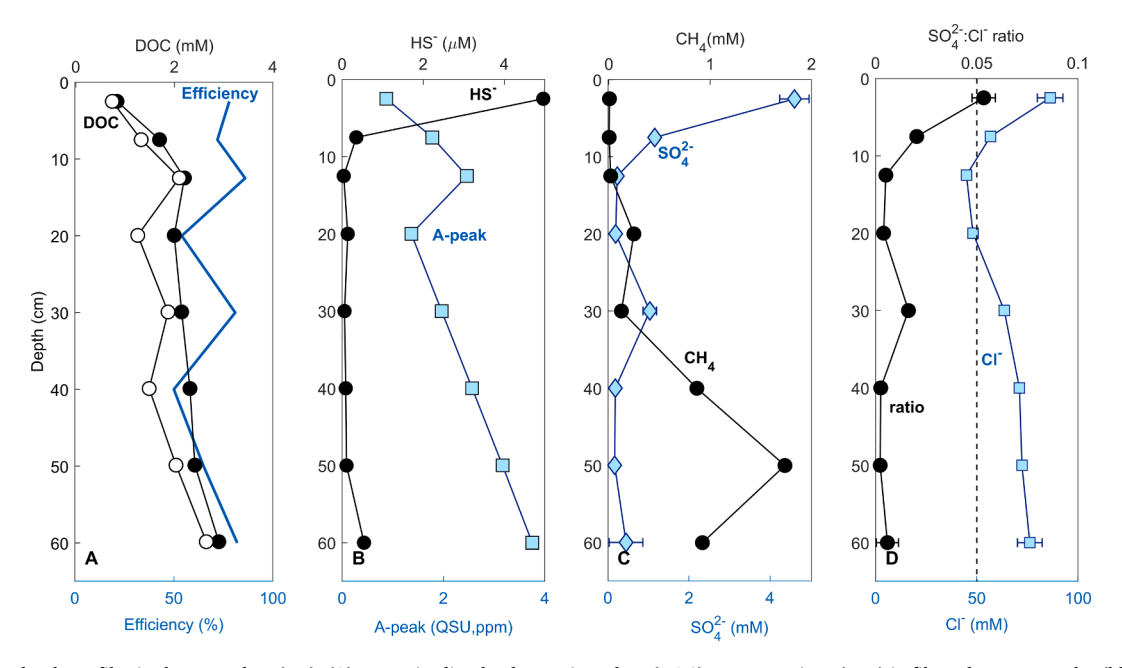


Fig. 1. Sediment depth profiles in the upper bay (UB). (A) Top axis: dissolved organic carbon (DOC) concentrations (mM) in filtered water samples (black circles) and SPE-PDOM samples (white circles). Bottom axis: DOC extraction efficiency (%) of SPE-PDOM samples (solid blue line). (B) Top axis: sulfide concentrations (HS $^-$, μ M) (black circles) and bottom axis: humic-like or A-peak fluorescence (blue squares) in quinine sulfate units (QSU, ppm). (C) Top axis: methane concentrations (CH $_4$, mM) (black circles) and bottom axis: sulfate concentrations (SO $_4$ 2 $^-$, mM) (blue diamonds). (D) Top axis: sulfate to chloride (CI $^-$) ratio (black circles) where the dashed line is at a SO $_4$ 2 $^-$:CI $^-$ ratio of 0.05 and represents conservative mixing of seawater with salinity greater than 2 as in ref. (Marvin-DiPasquale et al., 2003). Bottom axis: CI $^-$ concentrations (mM) (blue squares). (For interpretation of the references to colour in this figure legend, the reader is referred to the web version of this article.)

increased with depth (Supplementary Table S1, Fig. 1, Supplementary Figs. S1 and S2). There was also a discontinuity in the DOC, TDN, and NH₄ profiles at this station, which had elevated concentrations around 12 cm depth relative to the concentrations at \sim 20 cm sediment depth (Supplementary Table S1, Fig. 1, Supplementary Figs. S1 and S2). The shallow \sim 20 cm sediment may be subject to frequent resuspension

associated with the turbidity maximum (Schubel and Pritchard, 1986). Given the shallow water depth at UB (13 m), this site is prone to strong vertical mixing (Li et al., 2005) and it is possible the inflection in the data at 12 cm is due to an earlier event or hurricane (Sampere et al., 2008). On the other hand, because chloride concentrations also decreased between 10 cm and 20 cm at this site (Fig. 1), and submarine

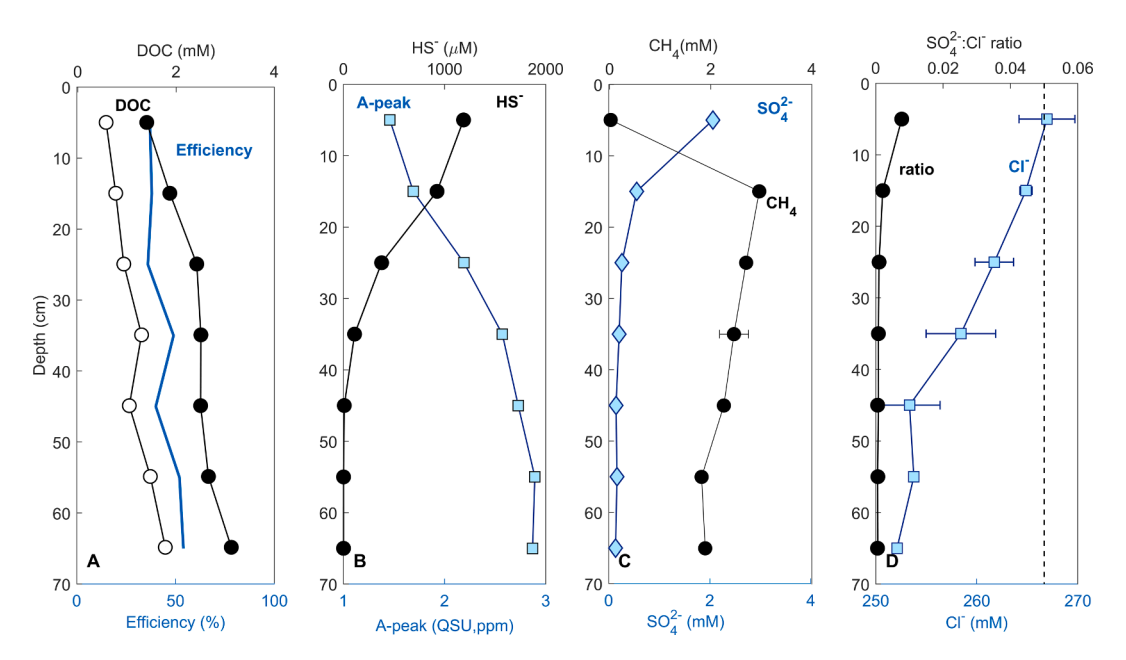


Fig. 2. Sediment depth profiles in the middle bay (MB). (A) Top axis: dissolved organic carbon (DOC) concentrations (mM) in filtered water samples (black circles) and SPE-PDOM samples (white circles). Bottom axis: DOC extraction efficiency (%) of SPE-PDOM samples (solid blue line). (B) Top axis: sulfide concentrations (HS $^-$, μ M) (black circles) and bottom axis: humic-like or A-peak fluorescence (blue squares) in quinine sulfate units (QSU, ppm). (C) Top axis: methane concentrations (CH4, mM) black circles and bottom axis: sulfate concentrations (SO $_4^{2-}$, mM) (blue diamonds). (D) Top axis: sulfate to chloride (Cl $^-$) ratio (black circles) where the dashed line is at a SO $_4^{2-}$:Cl $^-$ ratio of 0.05 and represents conservative mixing of seawater with salinity greater than 2 as in ref. (Marvin-DiPasquale et al., 2003). Bottom axis: Cl $^-$ concentrations (mM) (blue squares). (For interpretation of the references to colour in this figure legend, the reader is referred to the web version of this article.)

groundwater can be elevated in ammonium (Beck et al., 2016) (e.g., Supplementary Fig. S2), the inflections in the data might indicate lateral flow and the influence of groundwater. At the UB site, bottom waters are ventilated and bioturbating fauna are present. In surface sediments, animals irrigate biogenic structures with oxygenated bottom waters (i. e., bio-irrigation) and overturning sediment particles. These processes may play a significant role in the DOM cycling of surface sediments in the upper bay (Burdige, 2001). DOC was variable in the upper 5–10 cm at UB (Burdige, 2001) and model results indicate that the mixed-layer can extend down to about 10 cm in the upper bay (Nie et al., 2001). Therefore it is likely that bioturbation plays a role in the shaping the PDOM composition in the surface sediments at UB.

UB sulfate to chloride (SO₄²⁻:Cl⁻) molar ratios were below a conservative mixing value of 0.05, determined previously along a salinity gradient between 2 ppt and 36 ppt (Marvin-DiPasquale et al., 2003), at all depths except the surface (Supplementary Table S1, Fig. 1, Supplementary Fig. S1). However, hydrogen sulfide was $< 0.15 \mu M$ below 12 cm depth (Fig. 1), suggesting that bacterial sulfate reduction is very limited at UB. These observations are also consistent with previous work, which found low rates of sulfate reduction in upper bay sediments due to a limited sulfate supply (Marvin-DiPasquale et al., 2003) from low salinity (\sim 2–8 ppt) bottom waters (Shen et al., 2019). Additionally, hydrogen sulfide quickly reacts with a constant large supply of iron and reduced iron (Fe(II)) concentrations peaked at 340 µM in the 5-10 cm segment (Supplementary Fig. S2). Methane concentrations increased with depth, reaching 1.7 mM in the 50-60 cm segment (Fig. 1). Thus, sulfide may also be very low at UB due to high methane and Fe(II) concentrations that may result in the fast formation of iron monosulfides that are relatively stable in sediments with high concentrations of allochthonous DOM (Morgan et al., 2012).

DOC concentrations at MB increased continually with sediment depth and were similar in concentration to those at UB (Supplementary Table S2; Fig. 2). By contrast TDN concentrations increased more rapidly at MB than UB, resulting in a concentration an order of magnitude higher at ~60 cm depth at station MB compared to UB (Supplementary Table S2). Although we did not measure NH₄ at MB, this result suggests that inorganic nitrogen (possibly NH₄) concentrations must be much higher at MB than at UB. Previous work demonstrated that NH₄ fluxes from the mesohaline Chesapeake Bay sediments are highest in late summer, around the time of our sampling (Kemp et al., 1990). However, the TDN values measured here are well above DON + NH₄ measured in the mid bay during October sampling (Burdige and Zheng, 1998). This study reported mid bay DON concentrations of ~0.1 mM and NH₄ concentrations of ~2 mM at 20 cm, well below the 6.7 mM TDN measured in the 10-20 cm segment in this study. Inorganic N may be elevated in our MB samples since it has been suggested that centrifugation can lyse cells and cause nutrient release (Chen et al., 2015). However, TDN values at the UB site are in good agreement with NH₄ concentrations measured there (Supplementary Fig. S2), which at the very least indicates that there isn't major issue with the TDN measurements made in our study. Regardless, recent work revealed a strong correlation between NH4 concentrations and DON concentrations, and found evidence that ammonia production and accumulation of refractory DON can be explained by the deamination of peptides (Abdulla et al., 2018). Thus, TDN concentrations at MB could just be consistent with a source of very labile nitrogen-rich autochthonous DOM pool at this site (Zimmerman and Canuel, 2001).

Hydrogen sulfide was also much higher at station MB than UB, especially in the top 25 cm, with a maximum concentration of 1.2 mM near the surface (Supplementary Tables S1 and S2; Fig. 2). Similar sulfide concentrations (~1 mM) were observed in porewaters collected from the top 12 cm of sediment from the deep channel of the mid bay, which was accompanied by high rates of sulfate reduction (Hollweg et al., 2009). These results are expected because previous work has found that sulfate reduction dominates anaerobic organic carbon remineralization in the mid bay (Roden and Tuttle, 1993, 1996; Roden et al.,

1995; Marvin-DiPasquale et al., 2003). Sulfate depletion with depth in the top 30 cm is evident in both the SO_4^{2-} profile and the declining SO₄²⁻:Cl⁻ ratio profile (Fig. 2). Furthermore, methane concentrations were highest at 15 cm at MB and decreased slowly between 15 cm (3.0 mM) and 55 cm (1.8 mM) (Fig. 2). Therefore, in addition to organic matter dependent sulfate reduction, the depletion of sulfate and concomitant production of H2S could also be due to sulfate-dependent anaerobic oxidation of methane (Thang et al., 2013) given that CO₂ production is also very high at this site (Hollweg et al., 2009). Regardless of the dominant pathway, sulfide decreased rapidly below the sulfatemethane transition zone at about 20 cm (Fig. 2). In estuarine sediments of the Baltic Sea, where the sediment profiles were fairly similar, a large fraction of sulfur accumulated as pyrite and reduced organic sulfur (Thang et al. 2013). While we did not quantify pyrite, an accumulation of sulfur as reduced organic sulfur due to the reaction of H₂S with DOM is likely in the MB sediments (discussed in detail below).

3.2. Chemical properties of SPE-PDOM samples

DOC extraction efficiencies at UB were 65-86% except at 20 cm and 40 cm depths, where the extraction efficiency was 50-54%. Since the highest reported extraction efficiencies using this technique are ~75% (Dittmar et al., 2008; Stubbins et al., 2012), it is possible that our blank correction was not sufficient and the DOC was elevated in these SPE-PDOM samples potentially due to resin bleed, incomplete drying of methanolic extracts, or formic acid contamination due to our washing step. While these values should be interpreted with caution, since all extracts were treated in the same way, it is still worthwhile to note that the higher extraction efficiencies were achieved at UB when compared to MB. Extraction efficiencies at UB are also more in line with other terrestrial source materials and those at MB, 36-54%, are more similar to those for marine DOM (Dittmar et al., 2008). Even lower extraction efficiencies of only ~10% have been observed for freshly lysed algal DOM (Gonsior et al., 2019). Therefore, if the PDOM at MB is largely algal-derived, a lower DOC extraction efficiency would be expected.

At UB, SPE-PDOM concentrations generally increased with depth and a local decrease in SPE-DOC, SPE-DON, and SPE-DOS occurred at 20 cm (Supplementary Fig. S3). C:N ratios throughout the UB core ranged from 7.8 to 11 (Supplementary Table S1, Supplementary Fig. S4) and are in good agreement with the C:N ratios reported for Susquehanna River DOM (C:N = 9.3-11). (Hopkinson et al., 1998). However, it should be noted that these ratios may be season dependent or not entirely reflective of porewater DOM ratios, since previous work reported UB porewater DOM with variable DOC:DON ratios in the top ~20 cm, ranging from ~6-18 in March to ~12-26 in October (Burdige and Zheng, 1998). C:S ratios for UB SPE-PDOM samples were much higher than C:N ratios, ranging from 50 to 100. C:S values below 30 cm are more in line with those from \sim 50 to 85 reported for other porewaters in terrestrial sediments (Gomez-Saez et al., 2017; Ossola et al., 2019). However, terrestrial DOM and reference materials typically have much higher C:S ratios that are generally > 300 (Ossola et al., 2019). Like C:S ratios, N:S values generally decreased with depth at UB, demonstrating that there is a greater relative abundance of DOS at depth at this site (Supplementary Fig. S4). Decreasing C:S and N:S ratios could be explained by preferential preservation of DOS in UB sediments, given that a previous study suggested that low molecular weight (<1 kDa) DOS in terrestrial systems is largely refractory (Mitchell and Kang,

At MB, SPE-DOC and SPE-DON generally increased with depth, whereas SPE-DOS increased until 35 cm depth, after which SPE-DOS was relatively stable (Supplementary Table S2, Supplementary Fig. S3). Thus, C:N averaged 9.4 ± 1.0 whereas C:S increased with depth from 24 in the surface to 53 at depth and N:S increased with depth from 2.9 in the surface to 6.3 at depth (Supplementary Table S2, Supplementary Fig. S4). These C:S and N:S trends were the opposite of those at UB, but at comparative depths throughout the core, MB C:S ratios were well

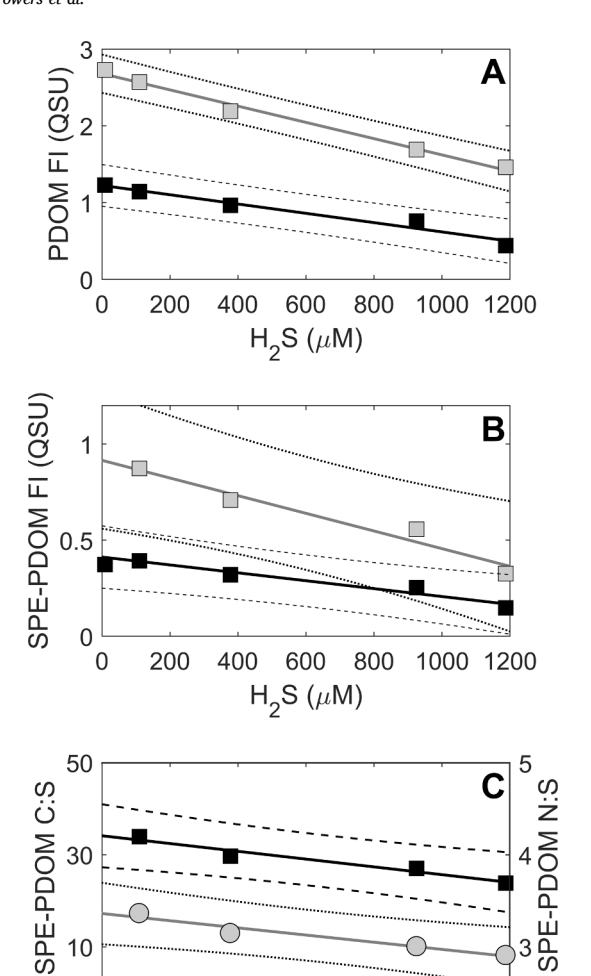


Fig. 3. Relationships between H_2S concentration and various properties at MB. (A) A-peak (gray squares) and C-peak (black squares) fluorescence intensity (FI, QSU) for porewater DOM (PDOM) vs H_2S concentration ($\mu M = \mu mole/L$). (B) A-peak (gray squares) and C-peak (black squares) fluorescence intensity (FI, QSU) for SPE-PDOM vs H_2S concentration (mM). In top and center plots solid gray lines are linear regressions between A-peak FI and H_2S and between C-peak and H_2S (dotted black lines are 95% confidence intervals, CI). Solid black lines are linear regressions between C-peak FI and H_2S (dashed black lines are 95 %CI). (C) C:S ratio of SPE-PDOM (black squares, left axis) and N:S ratio of SPE-PDOM (gray circles, right axis) vs H_2S concentration (μM). Here the solid black line is the linear regression between C:S and H_2S (dashed black lines are 95% CI) and the solid gray line is the linear regression between N:S and H_2S (dotted black lines are 95% CI).

600

 $H_2S(\mu M)$

800

1000 1200

400

0

0

200

below UB C:S ratios (Supplementary Fig. S4). C:S and N:S were 73% and 68% lower, respectively, in SPE-PDOM from MB surface sediments. At $\sim\!60$ cm depth, C:S and N:S were 30% and 6% lower, respectively. MB C: S and N:S also displayed inverse linear relationships with porewater sulfide concentrations in the top 35 cm of MB (Fig. 3). This C:S ratio could be predicted by the equation C:S = $-8.4 \times ([HS^-](mM)) + 34 \ (r^2 = 0.95, \ n = 4)$. Likewise, MB N:S ratios could be described by the equation $-0.39 \times ([HS^-](mM)) + 3.4 \ (r^2 = 0.94, \ n = 4)$ in the top 35 cm. While additional data are required to determine if these relationships are robust, a similar linear relationship between isolated DOM atomic C:S ratios and sulfide concentration has also been observed in the porewaters of sulfate impacted wetlands (Poulin et al., 2017). Although these trends are only based on a few samples, there was no correlation between C:S or N:S and sulfide in UB SPE-PDOM samples. The lower C:S and N:S ratios coinciding with higher sulfide concentrations at MB

strongly suggest that the sulfurization of PDOM (both in the DOC and DON pools) is occurring in the top \sim 40 cm at MB, at least during our sampling. At UB, sulfide concentrations are very low (Supplementary Table S1), limiting PDOM sulfurization. In the top 40 cm at UB, DOM composition is more likely controlled by bioturbation and other sediment remineralization processes (Burdige, 2001).

3.3. Fluorescence properties of sediment porewater in both the upper and mid bay

At UB, A and C fluorescence peaks (Equations (1) and (2)), generally increased with depth similarly with DOC/TDN concentrations, with a discontinuity observed in the top 20 cm, (Fig. 1, Supplementary Fig. S1). When normalized to DOC concentration, fluorescence intensity was variable in the top 20 cm, but progressively increased with depth below 20 cm (Supplementary Table S1, Supplementary Fig. S5). The variability in the top 20 cm may be attributed to bioturbation and the high and variable sedimentation rates at this site, as discussed above. The increase in humic-like fluorescence peaks in the profile at UB below 20 cm suggests that the FDOM pool is comprised of recalcitrant DOM that accumulates with depth. Like DOC concentrations. A-peak and C-peak fluorescence intensities at MB were on a similar scale to those at station UB (Fig. 1), even when normalized to DOC concentration (Supplementary Tables S1 and S2, Supplementary Fig. S5). These normalized fluorescence intensities fell in a narrower range when compared to those at UB. However, when plotted against DOC concentration, A-peak and Cpeak fluorescence intensities from both sites fell on the same regression line (Supplementary Fig. S5). While a strong relationship between Apeak fluorescence and DOC was previously shown in the mid bay for the top 25 cm (Burdige et al., 2004), our results highlight the convergence of fluorescence signals between contrasting UB and MB sediments.

Like SPE-PDOM C:S and N:S ratios, MB fluorescence intensities had an inverse linear relationship to hydrogen sulfide concentration in the upper 45 cm (Fig. 3), which was also not the case for these parameters at UB. Thus, A-peak fluorescence could be predicted by the equation A-peak(QSU) = $-1.06 \times ([HS^-](mM)) + 2.68 (r^2 = 0.99, n = 5)$ and C-peak fluorescence could be predicted by the equation C-peak(QSU) = $-0.605 \times ([HS^-](mM)) + 1.22 (r^2 = 0.96, n = 5)$. A previous study showed that during benthic chamber experiments, FDOM was produced in sediment cores during anoxic conditions (Skoog et al., 1996), which could explain the profile at MB and the inverse relationship to hydrogen sulfide. Furthermore, sulfate reduction has been linked to the production of DOM that has similar fluorescence properties to allochthonous or terrestrial DOM (Chen et al., 2016; Luek et al., 2017), which may also explain the relationship between HS $^-$ and A-peak/C-peak fluorescence at MB.

3.4. Fluorescence properties of SPE-PDOM samples

SPE-PDOM fluorescence intensities were higher at UB than at MB, even when normalized to SPE-DOC concentration (Supplementary Tables S1 and S2), which was not the case for porewater samples. The similarity in fluorescence intensities between sites in porewater samples may be due to matrix effects that were removed post SPE. For instance, some seawater cations, and in particular magnesium, may enhance DOM fluorescence signals (Stirchak et al., 2019) and pH differences between sites may also influence sample optical properties (Timko et al., 2015a; Schendorf et al., 2019). However, without measuring these properties directly, it is difficult to address their role in the sediment porewaters tested in this study. Intriguingly, despite the lower intensities at MB, SPE-PDOM EEM spectra displayed similar humic-like fluorescence features (Supplementary Fig. S6). There were, however, differences in spectral shape between the two sites and the difference in intensity between SPE-PDOM fluorescence in surface sediments (2.5-5 cm) and deep sediments (60-65 cm) was much smaller at the MB site when compared to the UB site (Supplementary Fig. S6). Thus, the differences

Table 1
Molecular characteristics of UB and MB SPE-PDOM at various depths determined from FT-ICR MS data. Intensity-weighted (wt) average molecular features described in the methods section are also listed.

Upper Bay depth (cm)	UB 5–10	UB 10–15	UB 15–25	UB 25–35	UB 35–45	UB 45–55	UB 55–65
CHO summed intensity	4.54×10^{10}	5.19×10^{10}	5.41×10^{10}	3.12×10^{10}	2.71×10^{10}	4.11×10^{10}	4.29×10^{10}
summed intensity (%)	75%	77%	76%	72%	67%	64%	69%
number CHO	1548	1453	1433	1462	1444	1449	1346
number CHO (%)	43%	43%	42%	44%	42%	37%	40%
Mass (Da)	353 ± 68	372 ± 60	383 ± 60	376 ± 63	392 ± 66	372 ± 66	405 ± 57
O/C _{wt}	0.50 ± 0.14	0.55 ± 0.13	0.56 ± 0.13	0.50 ± 0.13	0.48 ± 0.13	0.47 ± 0.13	0.50 ± 0.12
H/C _{wt}	1.11 ± 0.25	1.05 ± 0.24	1.06 ± 0.23	1.13 ± 0.23	1.17 ± 0.23	1.21 ± 0.24	1.14 ± 0.22
DBE_{wt}	8.5 ± 2.3	9.1 ± 2.3	9.2 ± 2.2	8.7 ± 2.3	8.8 ± 2.4	8.2 ± 2.4	9.2 ± 2.2
Cos_{wt}	-0.10 ± 0.42	0.04 ± 0.41	0.06 ± 0.41	-0.14 ± 0.40	-0.21 ± 0.40	-0.27 ± 0.40	-0.13 ± 0.38
CHOS summed intensity	3.81×10^{9}	3.03×10^{9}	3.13×10^{9}	2.77×10^{9}	3.43×10^{9}	6.71×10^{9}	4.82×10^{9}
summed intensity (%)	6%	5%	4%	6%	8%	10%	8%
number CHOS	435	413	411	403	473	614	522
number CHOS (%)	12%	12%	12%	12%	14%	16%	15%
Mass (Da)	326 ± 59	342 ± 63	352 ± 71	339 ± 61	359 ± 69	346 ± 63	392 ± 66
O/C _{wt}	0.42 ± 0.15	0.46 ± 0.15	0.48 ± 0.15	0.43 ± 0.15	0.44 ± 0.14	0.44 ± 0.14	0.49 ± 0.12
H/C _{wt}	1.56 ± 0.48	1.41 ± 0.50	1.35 ± 0.50	1.46 ± 0.48	1.36 ± 0.45	1.37 ± 0.41	1.18 ± 0.33
DBE _{wt}	$4.2 \pm 3.5 \ -0.57 \pm 0.71$	5.4 ± 3.9	$6.0 \pm 4.0 \ -0.25 \pm 0.72$	$5.2 \pm 3.9 \ -0.71 \pm 0.70$	$6.4 \pm 4.0 \\ -0.35 \pm 0.63$	$6.1 \pm 3.6 \ -0.36 \pm 0.61$	$8.2 \pm 3.2 \\ -0.07 \pm 0.48$
CUNO summed intensity	-0.57 ± 0.71 1.14×10^{10}	$-0.34 \pm 0.73 \\ 1.18 \times 10^{10}$	-0.25 ± 0.72 1.34×10^{10}	-0.71 ± 0.70 8.91×10^9	-0.35 ± 0.63 9.53×10^9	-0.36 ± 0.61 1.5×10^{10}	-0.07 ± 0.48 1.32×10^{10}
CHNO summed intensity summed intensity (%)	1.14 × 10 19%	1.18 × 10 18%	1.34 × 10 19%	8.91 × 10 21%	9.53 × 10 23%	23%	1.32 × 10 21%
number CHNO	1472	1406	1424	1344	1351	1527	1290
number CHNO (%)	41%	41%	42%	41%	39%	39%	38%
Mass (Da)	349 ± 66	368 ± 62	379 ± 62	369 ± 61	386 ± 63	366 ± 66	401 ± 56
O/C _{wt}	0.46 ± 0.12	0.49 ± 0.12	0.50 ± 0.11	0.46 ± 0.12	0.46 ± 0.11	0.46 ± 0.11	0.48 ± 0.10
H/C _{wt}	1.06 ± 0.12	1.05 ± 0.12	1.05 ± 0.21	1.08 ± 0.21	1.07 ± 0.11	1.17 ± 0.24	1.09 ± 0.19
DBE _{wt}	9.4 ± 2.4	9.7 ± 2.4	9.8 ± 2.4	9.6 ± 2.4	9.8 ± 2.3	8.8 ± 2.5	1.05 ± 0.15 10 ± 2.2
Cos _{wt}	0.14 ± 0.36	0.19 ± 0.34	0.21 ± 0.34	0.10 ± 0.33	0.05 ± 0.32	-0.01 ± 0.36	0.10 ± 0.31
CHNOS summed intensity	2.82×10^8	4.04×10^{8}	4.85×10^{8}	2.94×10^8	5.27×10^8	1.30×10^{9}	$1.2 imes 10^9$
summed intensity (%)	0.5%	0.6%	0.7%	0.7%	1.3%	2.0%	2.0%
number CHNOS	105	135	142	105	154	279	248
number CHNOS (%)	3%	4%	4%	3%	5%	7%	7%
Mass (Da)	320 ± 50	355 ± 53	370 ± 54	363 ± 42	384 ± 50	364 ± 57	400 ± 52
O/C _{wt}	0.49 ± 0.12	0.52 ± 0.11	0.52 ± 0.11	0.49 ± 0.09	0.49 ± 0.09	0.48 ± 0.11	0.49 ± 0.10
H/C _{wt}	1.06 ± 0.34	0.98 ± 0.31	0.97 ± 0.27	1.03 ± 0.22	1.04 ± 0.18	1.12 ± 0.20	1.05 ± 0.17
DBE_{wt}	$\textbf{7.8} \pm \textbf{2.7}$	9.1 ± 2.7	9.5 ± 2.6	9.0 ± 2.2	9.4 ± 2.2	8.4 ± 2.3	9.7 ± 2.1
Cos _{wt}	0.31 ± 0.46	$\textbf{0.40} \pm \textbf{0.45}$	0.42 ± 0.41	0.27 ± 0.31	0.25 ± 0.27	0.17 ± 0.32	0.23 ± 0.30
Mid Bay depth (cm)	MB 0–10	MB 10-20	MB 20-30	MB 30-40	MB 40–50	MB 50–60	MB 60–70
CHO summed intensity	1.01×10^{10}	2.45×10^{10}	2.58×10^{10}	3.25×10^{10}	3.26×10^{10}	5.12×10^{10}	4.61×10^{10}
CHO (%) intensity	51%	44%	46%	46%	47%	48%	51%
number CHO	1017	1186	1221	1260	1226	1318	1251
count (%)	31%	24%	25%	24%	25%	24%	25%
Mass (Da)	368 ± 79	371 ± 81	375 ± 78	371 ± 78	377 ± 75	372 ± 73	371 ± 74
O/C _{wt}	0.40 ± 0.09	0.39 ± 0.09	0.38 ± 0.09	0.38 ± 0.09	0.38 ± 0.08	0.39 ± 0.09	0.38 ± 0.08
H/C _{wt}	1.40 ± 0.22	1.42 ± 0.22	1.42 ± 0.21	1.42 ± 0.21	1.43 ± 0.20	1.42 ± 0.21	1.45 ± 0.19
DBE_{wt}	6.6 ± 2.2	6.5 ± 2.2	6.5 ± 2.2	6.5 ± 2.2	6.5 ± 2.1	6.5 ± 2.1	6.3 ± 2.0
Cos_{wt}	-0.60 ± 0.32	-0.64 ± 0.32	-0.66 ± 0.30	-0.65 ± 0.31	-0.66 ± 0.30	-0.64 ± 0.31	-0.69 ± 0.28
CHOS summed intensity	5.79×10^{9}	1.69×10^{10}	1.60×10^{10}	2.01×10^{10}	1.88×10^{10}	2.85×10^{10}	2.19×10^{10}
CHOS (%) intensity	30%	31%	29%	28%	27%	27%	24%
number CHOS	1013	1387	1328	1379	1317	1390	1283
count (%)	31%	29%	27%	27%	27%	26%	25%
Mass (Da)	368 ± 82	378 ± 83	382 ± 81	378 ± 82	386 ± 79	380 ± 77	381 ± 79
O/C _{wt}	0.40 ± 0.10	0.39 ± 0.09	0.39 ± 0.09	0.39 ± 0.09	0.40 ± 0.09	0.39 ± 0.10	0.39 ± 0.10
H/C _{wt}	1.53 ± 0.29	1.49 ± 0.26 5.4 ± 2.3	1.48 ± 0.24 5.6 ± 2.3	$1.50 \pm 0.26 \ 5.4 \pm 2.4$	1.49 ± 0.23 5.5 ± 2.2	1.50 ± 0.24	1.49 ± 0.21 5.6 ± 2.1
DBE _{wt}	5.1 ± 2.6				5.5 ± 2.2 -0.56 ± 0.32	5.4 ± 2.3	
Cos _{wt} CHNO	-0.58 ± 0.37 3.06×10^9	-0.56 ± 0.36 1.04×10^{10}	-0.57 ± 0.33 1.09×10^{10}	$\begin{array}{c} 0.57 \pm 0.35 \\ 1.43 \times 10^{10} \end{array}$	-0.36 ± 0.32 1.38×10^{10}	$-0.57 \pm 0.35 \ 2.21 imes 10^{10}$	-0.57 ± 0.30 1.84×10^{10}
CHNO (%) int	3.06 × 10 16%	1.04 × 10	20%	20%	20%	2.21 × 10 · · · · · · · · · · · · · · · · · ·	1.84 × 10
number CHNO	933	1570	20% 1645	20% 1787	20% 1647	1912	20% 1797
count (%)	29%	32%	34%	34%	34%	35%	36%
Mass (Da)	364 ± 71	374 ± 76	380 ± 74	379 ± 75	384 ± 71	382 ± 71	382 ± 74
O/C _{wt}	0.39 ± 0.09	0.38 ± 0.09	0.37 ± 0.09	0.38 ± 0.09	0.38 ± 0.09	0.38 ± 0.09	0.38 ± 0.09
H/C _{wt}	1.26 ± 0.22	1.27 ± 0.22	1.28 ± 0.22	1.27 ± 0.22	1.27 ± 0.21	1.27 ± 0.22	1.30 ± 0.22
DBE _{wt}	8.2 ± 2.3	8.3 ± 2.3	8.4 ± 2.4	8.5 ± 2.4	8.6 ± 2.3	8.6 ± 2.3	8.3 ± 2.4
Cos _{wt}	-0.20 ± 0.33	-0.23 ± 0.34	-0.25 ± 0.34	-0.24 ± 0.34	-0.24 ± 0.34	-0.22 ± 0.34	-0.27 ± 0.33
CHNOS summed int	6.90×10^{8}	3.39×10^{9}	3.22×10^{9}	4.05×10^9	3.63×10^{9}	5.60×10^9	4.44×10^9
CHNOS % (int)	4%	6%	6%	6%	5%	5%	5%
number CHNOS	274	703	686	755	678	772	719
count %	8%	15%	14%	15%	14%	14%	14%
Mass (Da)	370 ± 77	391 ± 82	396 ± 81	398 ± 83	400 ± 77	398 ± 78	399 ± 80
O/C _{wt}	0.40 ± 0.07	0.39 ± 0.08	0.39 ± 0.08	0.40 ± 0.08	0.40 ± 0.08	0.41 ± 0.09	0.40 ± 0.08
H/C _{wt}	1.31 ± 0.18	1.31 ± 0.21	1.32 ± 0.21	1.32 ± 0.21	1.32 ± 0.21	1.31 ± 0.21	1.34 ± 0.20
DBE _{wt}	7.1 ± 1.7	7.5 ± 2.0	7.5 ± 2.1	7.5 ± 2.1	$\textbf{7.5} \pm \textbf{2.1}$	$\textbf{7.5} \pm \textbf{2.1}$	$\textbf{7.4} \pm \textbf{2.1}$
Cos _{wt}	-0.18 ± 0.28	-0.20 ± 0.32	-0.23 ± 0.31	-0.20 ± 0.32	-0.21 ± 0.31	-0.18 ± 0.32	-0.23 ± 0.30

observed in SPE-PDOM fluorescence between sites are likely due to the very different organic matter provenance at these two locations.

At UB, A-peak/C-peak fluorescence in SPE-PDOM samples followed the same downcore trend as SPE-DOC (Supplementary Table S1) and generally increased. Like porewater samples, increases in fluorescence signals of SPE-PDOM with depth could reflect preservation of refractory terrestrial DOM at this site. Higher fluorescence values at the UB site may be due to the increasing importance of more aromatic and polyphenolic DOM with depth, because these molecular signatures typically correlate with humic-like FDOM (Stubbins et al., 2014). At the MB site, the inverse and linear relationships between sulfide concentrations and A-peak/C-peak fluorescence were still observed after SPE in the top 35 cm (Fig. 3). These equations had lower slopes than porewater samples and were A-peak(QSU) = $-0.460 \times ([HS^-](mM)) + 0.916 (r^2 = 0.95, n)$ = 4) and C-peak(QSU) = $-0.206 \times ([HS^-](mM)) + 0.412 (r^2 = 0.95, n)$ = 4). As expected, SPE-PDOM A-peak and C-peak fluorescence had direct correlations to C:S ratios and N:S ratios (A-peak(QSU) = $18 \times$ (C: S) + 17, r^2 = 0.98; C-peak(QSU) = 40 × (C:S) + 17, r^2 = 0.97, $r^$

peak(QSU) = $0.83 \times (N:S) + 2.6$, $r^2 = 0.94$; C-peak(QSU) = $1.8 \times (N:S) + 2.6$, $r^2 = 0.93$, n = 4). Despite these relationships, there is no way to know if sulfur-containing compounds contribute to humic-like fluorescence signals based on this current study alone. However, these results indicate that there are likely tight feedbacks between sulfate reduction, DOM sulfurization, and FDOM production in mid bay sediments (Chen et al., 2016; Luek et al., 2017).

3.5. Molecular diversity of porewater DOM analyzed by FT-ICR MS

As expected, the molecular composition of SPE-PDOM determined by FT-ICR MS revealed stark differences at all depths between station UB and MB (Table 1; Fig. 4). At station UB, formulas containing only carbon, hydrogen, and oxygen (CHO) were dominant (64–77% of total ion intensity), followed by those containing CHO plus nitrogen (CHNO) (18–23% of total ion intensity). There were also smaller pools of formulas containing CHO plus sulfur (CHOS) (4–10% of total ion intensity) and those containing CHNO plus sulfur (CHNOS) (0.5–2% of total ion

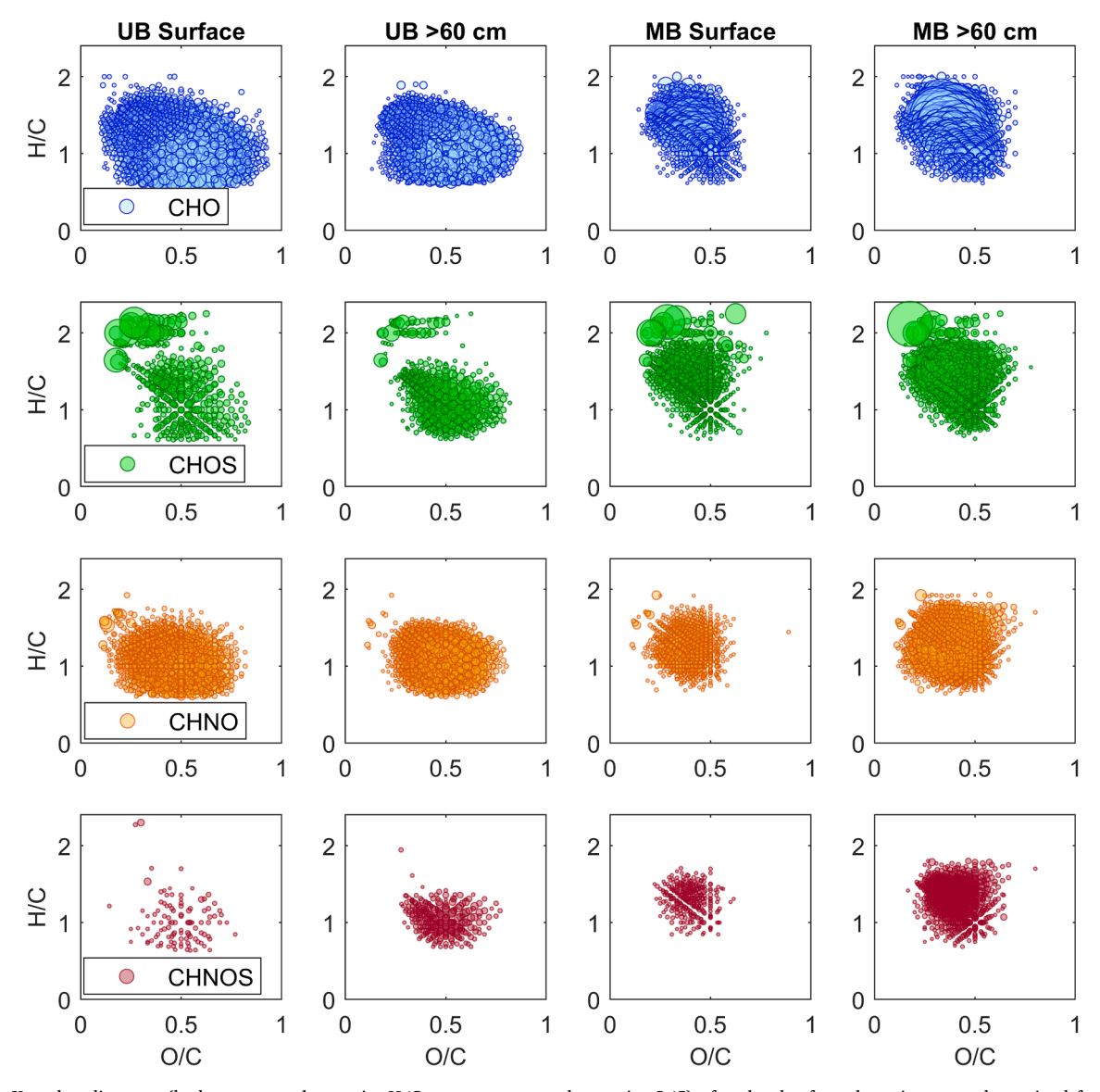


Fig. 4. Van Krevelen diagrams (hydrogen to carbon ratio, H/C, vs oxygen to carbon ratio, O/C) of molecular formula assignments determined for solid phase extracted sediment porewater DOM at station UB and MB as listed where columns 1 and 3 are from surface sediments (<10 cm depth) and columns 2 and 4 are from deep sediments (>60 cm depth). Formulas containing only carbon, hydrogen, and oxygen (CHO) are plotted in blue (top), those containing CHO + sulfur (CHOS) are plotted in green (second from top), and those containing CHO + nitrogen (CHNO) are plotted in orange (second from bottom) and those containing CHO + nitrogen and + sulfur (CHNOS) are plotted in red (bottom). For all diagrams, bubble size corresponds to ion intensity. (For interpretation of the references to colour in this figure legend, the reader is referred to the web version of this article.)

Table 2 Network analysis results testing H_2S addition reactions ($+H_2S=33.987721$ Da) between CHO precursors and CHOS products and between CHNO precursors and CHNOS products. Results for each site and depth are listed and both summed ion intensities (summed int) and number of ions, are compared. Percentages compare either summed intensities or number of ions between those in the network and those listed in Table 1.

Upper Bay depth (cm)	UB 5–10	UB 10–15	UB 15–25	UB 25–35	UB 35–45	UB 45–55	UB 55–65
CHO reacted (summed int)	2.19×10^{10}	2.34×10^{10}	2.27×10^{10}	1.42×10^{10}	1.23×10^{10}	1.89×10^{10}	1.82×10^{10}
% CHO reacted (summed int)	48%	45%	42%	46%	45%	46%	42%
number CHO reacted	435	432	428	427	418	428	393
% CHO reacted (number)	28%	30%	30%	29%	29%	30%	29%
CHOS reacted (summed int)	1.93×10^{9}	1.32×10^{9}	1.36×10^{9}	1.35×10^{9}	1.68×10^{9}	3.45×10^{9}	2.27×10^{9}
% CHOS reacted (summed int)	51%	44%	44%	49%	49%	51%	47%
number CHOS reacted	173	157	159	167	206	286	219
% CHOS reacted (number)	40%	38%	39%	41%	44%	47%	42%
CHNO reacted (summed int)	4.22×10^{9}	4.25×10^{9}	4.47×10^{9}	3.24×10^{9}	3.25×10^{9}	5.15×10^{9}	4.23×10^{9}
% CHNO reacted (summed int)	37%	36%	33%	36%	34%	34%	32%
number CHNO reacted	410	401	400	393	390	385	371
% CHNO reacted (number)	28%	29%	28%	29%	29%	25%	29%
CHNOS reacted (summed int)	1.12×10^8	1.66×10^{8}	2.16×10^8	1.43×10^{8}	2.66×10^{8}	6.87×10^{8}	6.15×10^{8}
% CHNOS reacted (summed int)	40%	41%	44%	49%	51%	53%	49%
number CHNOS reacted	39	54	59	48	77	140	121
% CHNOS reacted (number)	37%	40%	42%	46%	50%	50%	49%
Mid Bay depth (cm)	MB 0–10	MB 10–20	MB 20-30	MB 30-40	MB 40–50	MB 50-60	MB 60–70
CHO reacted (summed int)	4.01×10^{9}	9.46×10^{9}	1.00×10^{10}	1.27×10^{10}	1.28×10^{10}	2.03×10^{10}	1.80×10^{10}
% CHO reacted (summed int)	40%	39%	39%	39%	39%	40%	39%
number CHO reacted	337	361	371	376	367	389	373
% CHO reacted (number)	33%	30%	30%	30%	30%	30%	30%
CHOS reacted (summed int)	2.59×10^{9}	6.59×10^{9}	6.26×10^{9}	8.25×10^{9}	7.28×10^{9}	1.23×10^{10}	8.63×10^{9}
% CHOS reacted (summed int)	45%	39%	39%	41%	39%	43%	39%
number CHOS reacted	370	450	442	453	435	458	439
% CHOS reacted (number)	37%	32%	33%	33%	33%	33%	34%
CHNO reacted (summed int)	1.01×10^{9}	3.08×10^{9}	3.17×10^{9}	4.15×10^{9}	4.01×10^{9}	6.48×10^{9}	5.29×10^{9}
% CHNO reacted (summed int)	33%	30%	29%	29%	29%	29%	29%
number CHNO reacted	283	377	380	395	380	402	392
% CHNO reacted (number)	30%	24%	23%	22%	23%	21%	22%
CHNOS reacted (summed int)	3.83×10^{8}	1.81×10^{9}	1.80×10^{9}	2.20×10^{9}	2.07×10^{9}	3.17×10^{9}	2.37×10^{9}
% CHNOS reacted (summed int)	55%	53%	56%	54%	57%	57%	53%
number CHNOS reacted	159	359	379	395	379	415	370
% CHNOS reacted (number)	58%	51%	55%	52%	56%	54%	51%

intensity). The CHO and CHNO pools in particular showed a large diversity of molecular formulas that generally had high oxygenation with O/Cwt ranging 0.46-0.56 and high unsaturation with H/Cwt ranging from 1.05 to 1.21 (Table 1; Fig. 4), which is typical of aromatic DOM (Gonsior et al., 2016). At MB, the CHNO formulas had a similar average abundance (16-21% of ion intensities) as those at UB, but CHOS (24–31% of total ion intensity) and CHNOS (4–6% of total ion intensity) pools had much higher abundance. The CHO and CHNO pools at MB were very different from that at UB, exhibiting less oxygenation with O/ C_{wt} averaging 0.38 and higher saturation with H/C_{wt} averaging 1.43 for the CHO pool and 1.28 for the CHNO pool (Table 1; Fig. 4), which is more typical of algal DOM (Zhao et al., 2017; Gonsior et al., 2019). It should be noted that FT-ICR MS does not have sufficient sensitivity to depict small concentration changes in DOM constituents and intensities are highly dependent on how well compounds ionize using negative ESI. However, these generalizations are still useful in highlighting the very different molecular composition in extractable DOM between the upper and mid Chesapeake Bay sediment porewater.

At UB, the high abundance of CHO and CHNO formulas is consistent with FT-ICR MS data from terrestrially influenced porewaters (Seidel et al., 2014; Poulin et al., 2017), which exhibited a similar distribution in van Krevelen space (Fig. 4). Throughout the UB sediment core, average molecular characteristics do not change much with depth, but it is noteworthy that the abundance of CHOS and CHNOS was higher at 60 cm depth than at the surface (Table 1, Fig. 4), consistent with C:N, C:S, and N:S ratios discussed above. These results further support the preferential preservation of the DOS pool with depth at this site. Like CHO and CHNO pools, CHOS and CHNOS formulas generally occupied the same region of the van Krevelen diagram (Fig. 4) and showed similarities to CHOS formulas identified by FT-ICR MS in other terrestrially influenced sediments like river-impacted sediment porewaters (Schmidt et al., 2009), sulfidic wetland sediments (Poulin et al., 2017), tidal creek

porewaters (Seidel et al., 2014), and coastal porewater (Abdulla et al., 2020).

At MB, the comparatively high abundance of CHOS and CHNOS formulas is indicative of DOM sulfurization at this site and in good agreement with the generally lower C:S and N:S ratios observed here. It is also intriguing that the relative abundance of these pools did not increase with depth (Table 1), but this observation is also consistent with SPE-DOS concentrations. While intensity-weighted average characteristics often overlap between UB and MB (Table 1), it appears that the CHO and CHOS pools are fairly similar at all depths in MB sediments. For instance, mid bay CHO and CHOS had similar O/Cwt values around 0.40 and largely reduced COS_{wt} values (-0.55 to -0.65). CHOS H/C $_{wt}$ was slightly higher than CHO H/C_{wt} (1.50 for CHOS vs 1.43 for CHO) and DBE_{wt} was slightly lower (5.5 for CHOS vs 6.5 for CHO), which could indicate sulfurization of the CHO pool through Michael addition of sulfur to double bonds (Vairavamurthy and Mopper, 1987). However, the CHNOS pool had lower H/C_{wt} values and higher DBE_{wt} values when compared to the CHNO pool (Table 1). Therefore, using a network-based approach, a H2S addition reaction was tested between CHO and CHNO precursors and CHOS and CHNOS products, respectively, to better understand if this sulfurization reaction is predominant in MB porewaters.

3.6. Detailed comparisons of molecular composition by network analysis and hierarchical cluster analysis

Between UB and MB, the network analysis revealed that more molecular ions (e.g., 337–389 CHOS ions at MB vs 157–286 CHOS ions at UB) could be explained by H₂S addition reactions at MB (Table 2, Fig. 5). Summed CHOS ion intensities explained by H₂S addition were also much higher at MB (2.6–13 \times 10⁹) than at UB (1.3–3.5 \times 10⁹). Long homologous series spaced by CH₂ (horizontal) and +CH₄/–O (vertical) in modified Kendrick plots at MB indicate that CHOS and CHNOS pools at

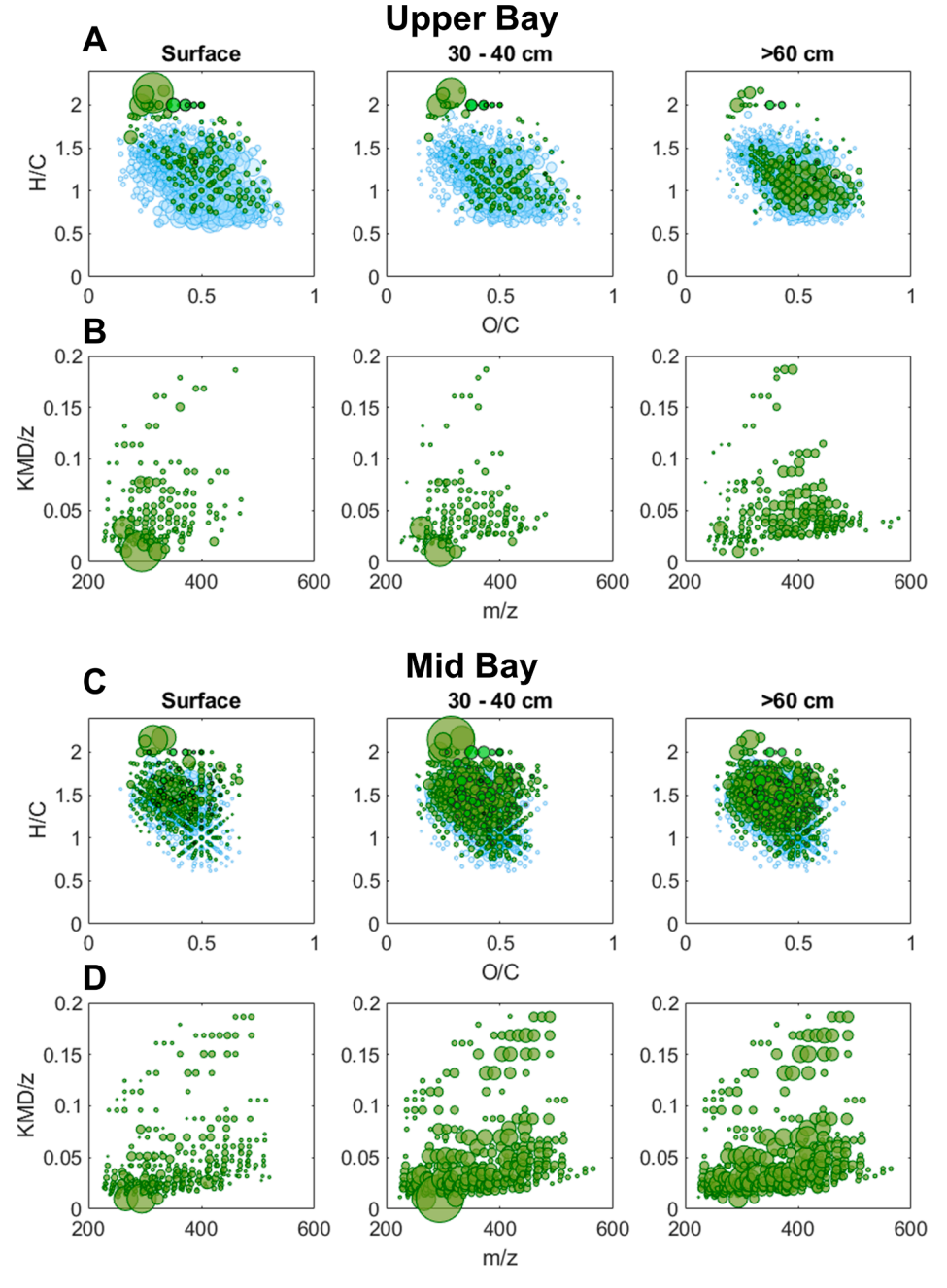


Fig. 5. Results of the network analysis between CHO precursors and CHOS products explained by H₂S addition reactions. (A) Van Krevelen diagrams of CHO (light blue circles), CHOS (green circles) and CHOS2 (neon green circles) linked by H2S in surface (\sim 0–10 cm, left), mid-depth (\sim 25–40 cm, center), and deep (~55-70 cm, left) UB sediments. (B) Modified Kendrick plots (KMD/ z^* vs m/z) of UB CHOS ions plotted in A) where same depths apply. (C) and (D) are analogous to (A) and (B), respectively, and depict the network analysis results for MB sediments. In all plots bubble size corresponds to ion intensity. (For interpretation of the references to colour in this figure legend, the reader is referred to the web version of this article.)

MB are highly related but those at UB are not (Fig. 5B, Supplementary Fig. S7). However, this finding is largely due to the much larger number of CHOS ions at MB when compared to UB (Table 1). In fact, H2S addition could explain 44-55% of the CHOS pool at UB and 39-45% of the CHOS pool at MB based on summed ion intensities (Table 2). In addition to the CHNOS pool being far more abundant at MB, H2S addition could explain 53-57% of the CHNOS formulas at MB and slightly less of the CHNOS formulas at UB (40-53%). These results are somewhat different from previous studies that found that sulfurization could explain ~64-70% of the CHOS pool detected in sediment porewater (Abdulla et al., 2020) and during reactions of seawater and phytoplankton DOM with sulfide (Pohlabeln et al., 2017). However, sulfur incorporation into the DOM pool under reducing conditions can be more complex than simple sulfide addition reactions. For instance, Pohlabeln et al. (2017) found evidence for several more complex sulfurization reactions, which included addition and losses of H2, H2O, and O₂ (Pohlabeln et al., 2017). We also tested several different sulfurization

reactions, e.g. $+H_2S/-H_2$, $+H_2S/-2H_2$, $+H_2S/-H_2O$, and $+H_2S/+H_2O/-2H_2$, which did not increase the proportion of the CHOS/CHNOS pools explained in our study. Therefore it is possible that the CHOS/CHNOS pools in this study are due to CHO/CHNO precursors that are absent or not visible using negative ESI-FT-ICR MS or are due to reaction mechanisms that are more complex than those tested here.

While up to \sim 50% of CHOS can be explained by sulfurization reactions, another explanation for the somewhat large number of CHOS that cannot be explained by H_2S addition is due to the presence of sulfonates that are already present in UB and MB sediment porewater. Because many known sulfonates would fall in the same region of the van Krevelen diagram (Figs. 4 and 5) and sulfonates ionize preferentially using ESI (Gonsior et al., 2011), their contribution to the CHOS pool cannot be ruled out. Sulfonic acids are also abundant in treated wastewater effluent that could enter the bay (Gonsior et al., 2011; Tseng et al., 2013), and these compounds may be relatively stable (Ossola et al., 2019). Sulfonates were also the dominant organosulfur species found in

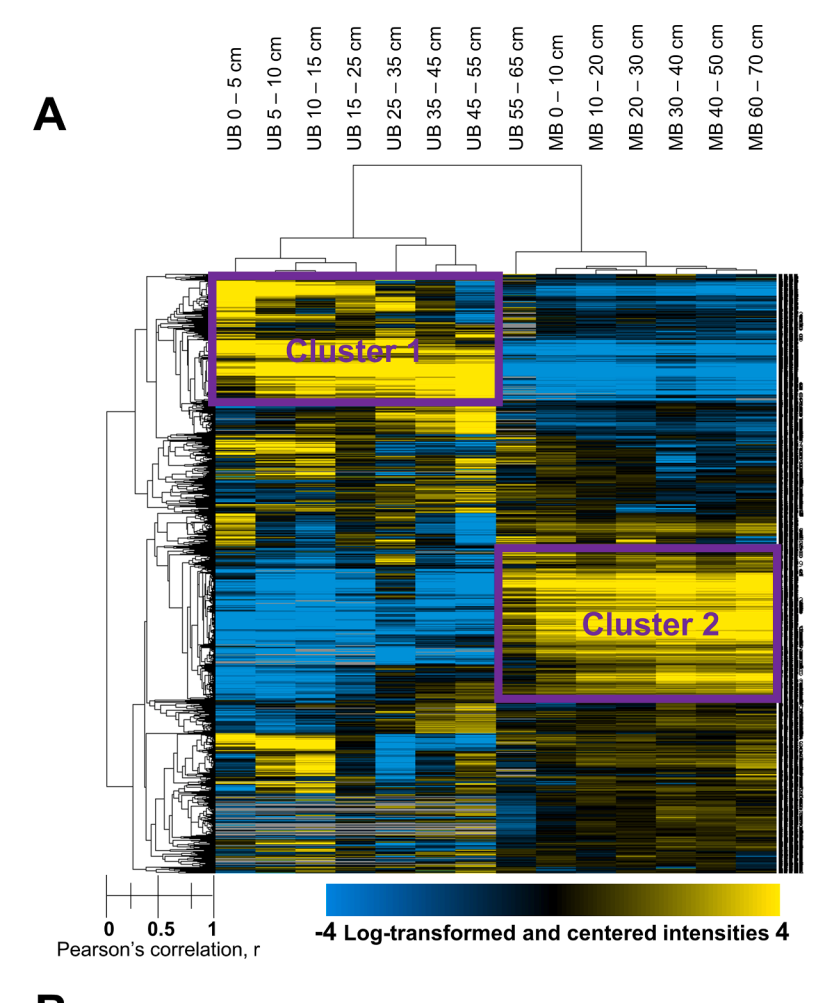
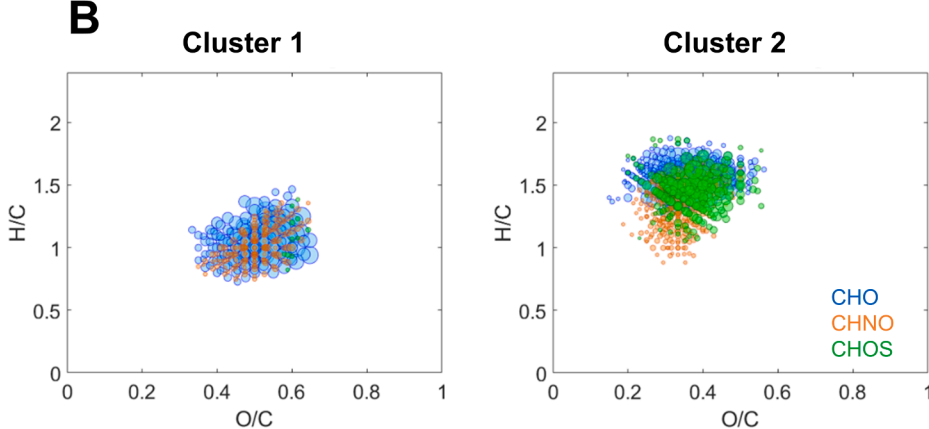


Fig. 6. (A) Two-dimensional hierarchical clustering of all log-transformed m/z ion intensities in the combined sample set of porewater DOM from station UB and MB at various sediment depths. The corresponding heat-map shows each m/z ion intensity as a row of colored rectangles for each depth segment and site (columns), using a scale that ranges from a log(intensity) of -4 (saturated blue) to log(intensity) of 4 (saturated yellow). Clusters were identified by Pearson's correlations from 0.5 to 1 and high ion intensities (yellow colors) at one site but not the other (blue colors). Highlighted in purple squares are cluster 1 and cluster 2, which depict indicative and high intensity m/z ions at station UB and at station MB, respectively. (B) Van Krevelen diagrams of ions in cluster 1 (left) and cluster 2 (right) where blue shows CHO ions, orange shows CHNO ions, and green shows CHOS ions and bubble size corresponds to ion intensity. (For interpretation of the references to colour in this figure legend, the reader is referred to the web version of this article.)



sediments of a similarly eutrophic temperate estuary of Western Australia (Morgan et al., 2012). On the other hand, previous work has shown that sulfonates can make up 20–40% of the organic sulfur in marine sediments, with the remaining 60–80% being reduced organic sulfur species (Vairavamurthy et al., 1994). Sulfurization of humic substances in sediments under reducing conditions has long been recognized as an important process in organic sulfur formation (Ferdelman et al., 1991). More recently, over 85% of the organic sulfur isolated from porewaters and analyzed by X-ray absorption spectroscopy was reduced (Poulin et al., 2017). Therefore, in order to better understand the dominant molecular ions at both sites, a two-dimensional hierarchical cluster analysis of all m/z ions was used to statistically compare the dominant molecular ions at the two stations (Fig. 6).

Indicative high intensity m/z ions for station UB (cluster 1) were

characterized by aromatic and highly unsaturated DOM, with H/C ratios ranging from ~0.8 to 1.4 (Fig. 6). Cluster 1 was also dominated by CHO and CHNO formulas and no CHOS formulas (Fig. 6), consistent with bulk DOM characterization at this site (Table 1). Another similar trend was that while there was some variability in ion intensities with depth, the vast majority of ions in cluster 1 were relatively stable throughout the sediment core (Fig. 6), perhaps reflecting the persistent nature of this material. On the other hand, indicative high intensity ions at MB (cluster 2 in Fig. 6) had almost no aromatic formulas (e.g., no assignments with high O/C ratios and low H/C ratios), which has been reported for algal DOM (Zhao et al., 2017; Gonsior et al., 2019). These molecular formulas had O/C ratios centered around 0.3 and only a small degree of unsaturation with H/C ratios ranging from 1.2 to 1.6 for CHO and CHOS assignments (Fig. 6). There was also a large CHOS pool in cluster 2 at MB,

which consisted of m/z ions in the molecular weight range of 300–500 Da (Supplementary Fig. S8). This CHOS pool was reduced, having low COS values ranging between -0.4 and -1.0 (Supplementary Fig. S8). Furthermore, homologous series spaced by only CH2 and O/C ratios always below 0.5 suggests that ions in the cluster 2 CHOS pool are highly related (Supplementary Fig. S8). Furthermore, ion intensities in cluster 2 increased with depth (Fig. 6), which was not obvious when analyzing the bulk CHOS pool (Table 1). While the caveat remains that ion intensities are not the same as concentration, CHOS increases were also observed in porewater of the Black Sea with similarly high (i.e., mM) sulfide concentrations (Schmidt et al., 2017). What is interesting is that while abundant CHOS pools have been observed in anoxic porewaters (Seidel et al., 2014; Abdulla et al., 2020), CHOS molecular formulas in these previous studies (Poulin et al., 2017; Abdulla et al., 2020) are more consistent with the sulfurization of a more diverse pool of compounds occupying a larger (and more aromatic) region of the van Krevelen diagram (Abdulla et al., 2020). Based on the relationship between C:S ratios and sulfide concentrations (Fig. 3C) and the similarity between CHO and CHOS formulas in the MB cluster (Fig. 6), the DOS pool at MB instead reflects the progressive sulfurization of algal-derived DOM.

Previous work has demonstrated that the DOS pool collected from sulfidic porewaters (Gomez-Saez et al., 2016) and from freshwater sources (Ossola et al., 2019) is largely photolabile when exposed to solar radiation, which is consistent with the idea that DOS may make a quantitatively significant contribution to the CDOM pool. We infer the sulfurization of DOM in sediments at MB most likely occurs by the addition of H₂S to double bonds (Vairavamurthy and Mopper, 1987), though other mechanisms such as the exchange of oxygen for sulfur cannot be ruled out (Hoffmann et al., 2012). Regardless of the dominant mechanism, sulfur additions should change sample optical properties given that oxygen is far more electronegative than sulfur. Chargetransfer interactions have been used to explain the optical properties of DOM (Sharpless and Blough, 2014), and sulfur is likely a better electron donor than oxygen (Pau et al., 1978). Furthermore, contrary to the rapid oxidation of thiols and thioethers, some reduced sulfur species (i.e., exocyclic and heterocyclic sulfur species) persist in oxygenated surface waters (Poulin et al., 2017) and the formation of S-heterocycles (i.e., thiophenes) during low-temperature reactions of polysulfides with carbonyl-containing compounds has been documented (LaLonde et al., 1987; Rowland et al., 1993). Previous work found abundant pyrrolic (Nheterocycle) ring structures in DOM from picocyanobacteria and suggested their involvement in the fluorescent DOM pool (Zhao et al., 2017). Along the same lines, many thiophene based compounds exhibit fluorescent properties, especially bithiophene and dithieno-pyrrolic compounds (Rasmussen et al., 2015). Currently, more work is needed to characterize the DOS pool in various environments to better understand its formation mechanisms and to decipher fluorophores tightly coupled to sulfate reduction.

4. Conclusions

PDOM of the upper bay was highly oxygenated and aromatic in nature, which likely reflects the polyphenolic composition of terrestrially derived DOM. In contrast, the molecular composition of the PDOM pool in the mid bay was less oxygenated and more saturated, and likely derived from cyanobacterial and algal DOM. A strong inverse correlation between A-peak/C-peak fluorescence and hydrogen sulfide concentration was also found in the mid bay sediment depth profile. This relationship suggests a link between increases in humic-like fluorescence and sulfate reduction at this site. Furthermore, the mid bay CHOS pool progressively increased with depth and was non-aromatic in nature, suggesting an addition reaction of hydrogen sulfide to unsaturated organic molecules derived from algae. Our results support the idea that algal-derived DOM and its transformations can have fluorescence features similar to terrestrial materials.

Declaration of Competing Interest

The authors declare that they have no known competing financial interests or personal relationships that could have appeared to influence the work reported in this paper.

Acknowledgements

We thank the captain and crew of the R/V Rachel Carson for assistance in collecting sediment cores. Funding for this work was supported by Horn Point Laboratory start-up funds and the National Science Foundation [grant number OCE-1756877] to Sairah Malkin and the American Chemical Society Petroleum Research Fund [grant number 54849-DNI2] to Michael Gonsior. We also would like to thank the editors and two anonymous reviewers for their thoughtful comments that helped improve this manuscript. This is contribution No. 6053 and Ref. No. [UMCES] CBL 2022-013 of the University of Maryland Center for Environmental Science.

Data availability

All data associated with this study are available in the main text or in supplementary tables and figures. FT-ICR MS data have been submitted to the PANGAEA database (PDI-29322, https://www.pangaea.de/). All other data are available by request from the corresponding authors.

Appendix A. Supplementary material

Supplementary data to this article can be found online at https://doi.org/10.1016/j.orggeochem.2021.104324.

References

- Abdulla, H.A., Burdige, D.J., Komada, T., 2018. Accumulation of deaminated peptides in anoxic sediments of Santa Barbara Basin. Geochimica et Cosmochimica Acta 223, 245–258.
- Abdulla, H.A., Burdige, D.J., Komada, T., 2020. Abiotic formation of dissolved organic sulfur in anoxic sediments of Santa Barbara Basin. Organic Geochemistry 139, 102270.
- Bauer, J.E., Cai, W.-J., Raymond, P.A., Bianchi, T.S., Hopkinson, C.S., Regnier, P.A.G., 2013. The changing carbon cycle of the coastal ocean. Nature 504, 61–70.
- Beck, A.J., Kellum, A.A., Luek, J.L., Cochran, M.A., 2016. Chemical flux associated with spatially and temporally variable submarine groundwater discharge, and chemical modification in the subterranean estuary at Gloucester Point, VA (USA). Estuaries and Coasts 39, 1–12.
- Boyle, E.S., Guerriero, N., Thiallet, A., Del Vecchio, R., Blough, N.V., 2009. Optical properties of humic substances and CDOM: Relation to structure. Environmental Science and Technology 43, 2262–2268.
- Brüchert, V., 1998. Early diagenesis of sulfur in estuarine sediments: the role of sedimentary humic and fulvic acids. Geochimica et Cosmochimica Acta 62, 1567–1586.
- Burdige, D.J., 2001. Dissolved organic matter in Chesapeake Bay sediment pore waters. Organic Geochemistry 32, 487–505.
- Burdige, D.J., Homstead, J., 1994. Fluxes of dissolved organic carbon from Chesapeake Bay sediments. Geochimica et Cosmochimica Acta 58, 3407–3424.
- Burdige, D.J., Kline, S.W., Chen, W., 2004. Fluorescent dissolved organic matter in marine sediment pore waters. Marine Chemistry 89, 289–311.
- Burdige, D.J., Zheng, S., 1998. The biogeochemical cycling of dissolved organic nitrogen in estuarine sediments. Limnology and Oceanography 43, 1796–1813.
- Chen, M., Kim, J.-H., Nam, S.-I., Niessen, F., Hong, W.-L., Kang, M.-H., Hur, J., 2016. Production of fluorescent dissolved organic matter in Arctic Ocean sediments. Scientific Reports 6, 39213.
- Chen, M., Lee, J.H., Hur, J., 2015. Effects of sampling methods on the quantity and quality of dissolved organic matter in sediment pore waters as revealed by absorption and fluorescence spectroscopy. Environmental Science and Pollution Research 22, 14841–14851.
- Clark, C.D., de Bruyn, W., Jones, J.G., 2014. Photoproduction of hydrogen peroxide in aqueous solution from model compounds for chromophoric dissolved organic matter (CDOM). Marine Pollution Bulletin 79, 54–60.
- Cline, J.D., 1969. Spectrophotometric determination of hydrogen sulfide in natural waters. Limnology and Oceanography 14, 454–458.
- Coble, P.G., 1996. Characterization of marine and terrestrial DOM in seawater using excitation-emission matrix spectroscopy. Marine Chemistry 51, 325–346.
- D'Andrilli, J.D., Chanton, J.P., Glaser, P.H., Cooper, W.T., 2010. Characterization of dissolved organic matter in northern peatland soil porewaters by ultra high resolution mass spectrometry. Organic Geochemistry 41, 791–799.

- De Graaf, W., Sinninghe Damsté, J.S., de Leeuw, J.W., 1992. Laboratory simulation of natural sulphurization: I. Formation of monomeric and oligomeric isoprenoid polysulphides by low-temperature reactions of inorganic polysulphides with phytol and phytadienes. Geochimica et Cosmochimica Acta 56, 4321–4328.
- Derrien, M., Lee, Y.K., Shin, K.H., Hur, J., 2018. Comparing discrimination capabilities of fluorescence spectroscopy vs FT-ICR-MS for sources and hydrophobicity of sediment organic matter. Environmental Science and Pollution Research 25, 1892–1902.
- Dittmar, T., Koch, B., Hertkorn, N., Kattner, G., 2008. A simple and efficient method for the solid-phase extraction of dissolved organic matter (SPE-DOM) from seawater. Limnology and Oceanography: Methods 6, 230–235.
- Eisen, M.B., Spellman, P.T., Brown, P.O., Botstein, D., 1999. Cluster analysis and display of genome-wide expression patterns. Proceedings of the National Academy of Science 95, 14836–14868.
- Ferdelman, T.G., Church, T.M., Luther, G.W., 1991. Sulfur enrichment of humic substances in a Delaware salt marsh sediment core. Geochimica et Cosmochimica Acta 55, 979–988.
- Francois, R., 1987. A study of sulfur enrichment in the humic fraction of marinesediments during early diagenesis. Geochimica et Cosmochimica Acta 51, 17–27.
- Gomez-Saez, G.V., Niggemann, J., Dittmar, T., Pohlabeln, A.M., Lang, S.Q., Noowong, A., Pichler, T., Wörmer, L., Bühring, S.I., 2016. Molecular evidence for abiotic sulfurization of dissolved organic matter in marine shallow hydrothermal systems. Geochimica et Cosmochimica Acta 190, 35–52.
- Gomez-Saez, G.V., Pohlabeln, A.M., Stubbins, A., Marsay, C.M., Dittmar, T., 2017.
 Photochemical alteration of dissolved organic sulfur from sulfidic porewater.
 Environmental Science & Technology 51, 14144–14154.
- Gonsior, M., Powers, L.C., Williams, E., Place, A., Chen, F., Ruf, A., Hertkorn, N., Schmitt-Kopplin, P., 2019. The chemodiversity of algal dissolved organic matter from lysed *Microcystis aeruginosa* cells and its ability to form disinfection by-products during chlorination. Water Research 155, 300–309.
- Gonsior, M., Zwartjes, M., Cooper, W.J., Song, W., Ishida, K.P., Tseng, L.Y., Jeung, M.K., Rosso, D., Hertkorn, N., Schmitt-Kopplin, P., 2011. Molecular characterization of effluent organic matter identified by ultrahigh resolution mass spectrometry. Water Research 45, 2943–2953.
- Gonsior, M., Valle, J., Schmitt-Kopplin, P., Hertkorn, N., Bastviken, D., Luek, J., Harir, M., Bastos, W., Enrich-Prast, A., 2016. Chemodiversity of dissolved organic matter in the Amazon Basin. Biogeosciences 13, 4279–4290.
- He, W., Jung, H., Lee, J.H., Hur, J., 2016. Differences in spectroscopic characteristics between dissolved and particulate organic matters in sediments: Insight into distribution behavior of sediment organic matter. Science of the Total Environment 547. 1–8.
- Heitmann, T., Blodau, C., 2006. Oxidation and incorporation of hydrogen sulfide by dissolved organic matter. Chemical Geology 235, 12–20.
- Helder, W., De Vries, R.T.P., 1979. An automatic phenol-hypochlorite method for the determination of ammonia in sea- and brackish waters. Netherlands Journal of Sea Research 13, 154–160.
- Hernes, P.J., Spencer, R.G.M., Dyda, R.Y., Pellerin, B.A., Bachand, P.A.M., Bergamaschi, B.A., 2008. The role of hydrologic regimes on dissolved organic carbon composition in an agricultural watershed. Geochimica et Cosmochimica Acta 72, 5266–5277.
- Herzsprung, P., Hertkorn, N., von Tümpling, W., Harir, M., Friese, K., Schmitt-Kopplin, P., 2014. Understanding molecular formula assignment of Fourier transform ion cyclotron resonance mass spectrometry data of natural organic matter from a chemical point of view. Analytical and Bioanalytical Chemistry 406, 7977–7987.
- Herzsprung, P., Tümpling, W.V., Wendt-Potthoff, K., Hertkorn, N., Harir, M., Schmitt-Kopplin, P., Friese, K., 2017. High field FT-ICR mass spectrometry data sets enlighten qualitative DOM alteration in lake sediment porewater profiles. Organic Geochemistry 108. 51–60.
- Hoffmann, M., Mikutta, C., Kretzschmar, R., 2012. Bisulfide reaction with natural organic matter enhances arsenite sorption: Insights from X-ray absorption spectroscopy. Environmental Science and Technology 46, 11788–11797.
- Hollweg, T.A., Gilmour, C.C., Mason, R.P., 2009. Methylmercury production in sediments of Chesapeake Bay and the mid-Atlantic continental margin. Marine Chemistry 114, 86–101.
- Hopkinson, C.S., Buffam, I., Hobbie, J., Vallino, J., Perdue, M., Eversmeyer, B., Prahl, F., Covert, J., Hodson, R., Moran, M.A., Smith, E., Baross, J., Crump, B., Findlay, S., Foreman, K., 1998. Terrestrial inputs of organic matter to coastal ecosystems: An intercomparison of chemical characteristics and bioavailability. Biogeochemistry 43, 211–234.
- Kemp, W.M., Sampou, P., Caffrey, J., Mayer, M., Henriksen, K., Boynton, W.R., 1990. Ammonium recycling vs denitrification in Chesapeake Bay sediments. Limnology and Oceanography 35, 1545–1563.
- Kendrick, E., 1963. A mass scale based on $CH_2=14.0000$ for high resolution mass spectrometry of organic compounds. Analytical Chemistry 35, 2146–2154.
- Kida, M., Fujitake, N., Kojima, T., Tanabe, Y., Hayashi, K., Kudoh, S., Dittmar, T., 2021. Dissolved organic matter processing in pristine Antarctic streams. Environmental Science & Technology 55, 10175–10185.
- Kida, M., Kojima, T., Tanabe, Y., Hayashi, K., Kudoh, S., Maie, N., Fujitake, N., 2019. Origin, distributions, and environmental significance of ubiquitous humic-like fluorophores in Antarctic lakes and streams. Water Research 163, 114901.
- Koch, B.P., Dittmar, T., 2006. From mass to structure: An aromaticity index for highresolution mass data of natural organic matter. Rapid Communications in Mass Spectrometry 20, 926–932.
- Koch, B.P., Dittmar, T., Witt, M., Kattner, G., 2007. Fundamentals of molecular formula assignment to ultrahigh resolution mass data of natural organic matter. Analytical Chemistry 79, 1758–1763.

- Kroll, J.H., Donahue, N.M., Jimenez, J.L., Kessler, S.H., Canagaratna, M.R., Wilson, K.R., Altieri, K.E., Mazzoleni, L.R., Wozniak, A.S., Bluhm, H., Mysak, E.R., Smith, J.D., Kolb, C.E., Worsnop, D.R., 2011. Carbon oxidation state as a metric for describing the chemistry of atmospheric organic aerosol. Nature Chemistry 3, 133–139.
- Ksionzek, K.B., Lechtenfeld, O.J., McCallister, S.L., Schmitt-Kopplin, P., Geuer, J.K., Geibert, W., Koch, B.P., 2016. Dissolved organic sulfur in the ocean: Biogeochemistry of a petagram inventory. Science 354, 456–459.
- LaLonde, R.T., Ferrara, L.M., Hayes, M.P., 1987. Low-temperature, polysulfide reactions of conjugated ene carbonyls: A reaction model for the geologic origin of Sheterocycles. Organic Geochemistry 11, 563–571.
- Larsson, T., Wedborg, M., Turner, D., 2007. Correction of inner-filter effect in fluorescence excitation-emission matrix spectrometry using Raman scatter. Analytica Chimica Acta 583, 357–363.
- Li, M., Zhong, L., Boicourt, W.C., 2005. Simulations of Chesapeake Bay estuary: Sensitivity to turbulence mixing parameterizations and comparison with observations. Journal of Geophysical Research 110, 1–22.
- Lucio, M., 2009. Datamining metabolomics: the convergence point of non-target approach and statistical investigation. Technische Universität München.
- Luek, J.L., Thompson, K.E., Larsen, R.K., Heyes, A., Gonsior, M., 2017. Sulfate reduction in sediments produces high levels of chromophoric dissolved organic matter. Scientific Reports 7, 1–8.
- Luther, G.W., Giblin, A.E., Varsolona, R., 1985. Polarographic analysis of sulfur species in marine porewaters. Limnology and Oceanography 30, 727–736.
- Martin, W.R., McCorkle, D.C., 1993. Dissolved organic carbon concentrations in marine pore waters determined by high-temperature oxidation. Limnology and Oceanography 38, 1464–1479.
- Marvin-DiPasquale, M.C., Boynton, W.R., Capone, D.G., 2003. Benthic sulfate reduction along the Chesapeake Bay central channel. II. Temporal controls. Marine Ecology Progress Series 260, 55–70.
- Mitchell, M.J., Kang, P.-G., 2013. Bioavailability and size-fraction of dissolved organic carbon, nitrogen, and sulfur at the Arbutus Lake watershed, Adirondack Mountains, NY. Biogeochemistry 115, 213–234.
- Morgan, B., Burton, E.D., Rate, A.W., 2012. Iron monosulfide enrichment and the presence of organosulfur in eutrophic estuarine sediments. Chemical Geology 296–297, 119–130.
- Murphy, K.R., Butler, K.D., Spencer, R.G.M., Stedmon, C.A., Boehme, J.R., Aiken, G.R., 2010. Measurement of dissolved organic matter fluorescence in aquatic environments: An interlaboratory comparison. Environmental Science and Technology 44, 9405–9412.
- Nelson, N.B., Siegel, D.A., 2013. The global distribution and dynamics of chromophoric dissolved organic matter. Annual Review of Marine Science 5, 447–476.
- Nelson, N.B., Siegel, D.A., Carlson, C.A., Swan, C., Smethie, W.M., Khatiwala, S., 2007. Hydrography of chromophoric dissolved organic matter in the North Atlantic. Deep Sea Research Part I: Oceanographic Research Papers 54, 710–731.
- Nelson, N.B., Siegel, D.A., Michaels, A.F., 1998. Seasonal dynamics of colored dissolved material in the Sargasso Sea. Deep-Sea Research Part I: Oceanographic Research Papers 45, 931–957.
- Nie, Y., Suayah, I.B., Benninger, L.K., Alperin, M.J., 2001. Modeling detailed sedimentary ²¹⁰Pb and fallout ^{239,240}Pu profiles to allow episodic events: An application in Chesapeake Bay. Limnology and Oceanography 46, 1425–1437.
- Ossola, R., Tolu, J., Clerc, B., Erickson, P.R., Winkel, L.H.E., Mcneill, K., 2019.

 Photochemical production of sulfate and methanesulfonic acid from dissolved organic sulfur in natural waters. Environmental Science & Technology 53, 13191–13200.
- Osterholz, H., Kirchman, D.L., Niggemann, J., Dittmar, T., 2016. Environmental drivers of dissolved organic matter molecular composition in the Delaware Estuary. Frontiers in Earth Science 4, 1–6.
- Pau, J.K., Ruggera, M.B., Kim, J.K., Caserio, M.C., 1978. On the electron-donating properties of oxygen vs. sulfur. A study of the gas-phase ion chemistry of methoxymethylthioalkanes. Journal of the American Chemical Society 100, 4242–4248.
- Peterson, B.J., Howarth, R.W., 1987. Sulfur, carbon, and nitrogen isotopes used to trace organic matter flow in the salt-marsh estuaries of Sapelo Island, Georgia. Limnology and Oceanography 32, 1195–1213.
- Pohlabeln, A.M., Gomez-Saez, G.V., Noriega-Ortega, B.E., Dittmar, T., 2017. Experimental evidence for abiotic sulfurization of marine dissolved organic matter. Frontiers in Marine Science 4, 1–11.
- Poulin, B.A., Ryan, J.N., Nagy, K.L., Stubbins, A., Dittmar, T., Orem, W., Krabbenhoft, D. P., Aiken, G.R., 2017. Spatial dependence of reduced sulfur in Everglades dissolved organic matter controlled by sulfate enrichment. Environmental Science and Technology 51, 3630–3639.
- Powers, L.C., Luek, J.L., Schmitt-Kopplin, P., Campbell, B.J., Magen, C., Cooper, L.W., Gonsior, M., 2018. Seasonal changes in dissolved organic matter composition in Delaware Bay, USA in March and August 2014. Organic Geochemistry 122, 87–97.
- Rasmussen, S.C., Evenson, S.J., McCausland, C.B., 2015. Fluorescent thiophene-based materials and their outlook for emissive applications. Chemical Communications 51, 4528–4543.
- Roden, E.E., Tuttle, J.H., 1993. Inorganic sulfur cycling in mid and lower Chesapeake Bay sediments. Marine Ecology Progress Series 93, 101–118.
- Roden, E.E., Tuttle, J.H., 1996. Carbon cycling in mesohaline Chesapeake Bay sediments 2: Kinetics of particulate and dissolved organic carbon turnover. Journal of Marine Research 54, 343–383.
- Roden, E.E., Tuttle, J.H., Boynton, W.R., Kemp, W.M., 1995. Carbon cycling in mesohaline Chesapeake Bay sediments 1: POC deposition rates and mineralization pathways. Journal of Marine Research 53, 799–819.

- Rossel, P.E., Bienhold, C., Boetius, A., Dittmar, T., 2016. Dissolved organic matter in pore water of Arctic Ocean sediments: Environmental influence on molecular composition. Organic Geochemistry 97, 41–52.
- Rowland, S., Rockey, C., Al-Lihaibi, S.S., Wolff, G.A., 1993. Incorporation of sulphur into phytol derivatives during simulated early diagenesis. Organic Geochemistry 20, 1–5.
- Saldanha, A.J., 2004. Java Treeview Extensible visualization of microarray data. Bioinformatics 20, 3246–3248.
- Sampere, T.P., Bianchi, T.S., Wakeham, S.G., Allison, M.A., 2008. Sources of organic matter in surface sediments of the Louisiana Continental margin: Effects of major depositional/transport pathways and Hurricane Ivan. Continental Shelf Research 28, 2472–2487.
- Schendorf, T.M., Del Vecchio, R., Bianca, M., Blough, N.V., 2019. Combined effects of pH and borohydride reduction on optical properties of humic substances (HS): A comparison of optical models. Environmental Science and Technology 53, 6310–6319.
- Schmidt, F., Elvert, M., Koch, B.P., Witt, M., Hinrichs, K.U., 2009. Molecular characterization of dissolved organic matter in pore water of continental shelf sediments. Geochimica et Cosmochimica Acta 73, 3337–3358.
- Schmidt, F., Koch, B.P., Goldhammer, T., Elvert, M., Witt, M., Lin, Y.S., Wendt, J., Zabel, M., Heuer, V.B., Hinrichs, K.U., 2017. Unraveling signatures of biogeochemical processes and the depositional setting in the molecular composition of pore water DOM across different marine environments. Geochimica et Cosmochimica Acta 207, 57–80.
- Schmidt, F., Koch, B.P., Elvert, M., Schmidt, G., Witt, M., Hinrichs, K.U., 2011. Diagenetic transformation of dissolved organic nitrogen compounds under contrasting sedimentary redox conditions in the black sea. Environmental Science and Technology 45, 5223–5229.
- Schouten, S., van Driel, G.B., Sinninghe Damsté, J.S., de Leeuw, J.W., 1993. Natural sulphurization of ketones and aldehydes: A key reaction in the formation of organic sulphur compounds. Geochimica et Cosmochimica Acta 57, 5111–5116.
- Schouten, S., de Graaf, W., Sinninghe Damsté, J.S., van Driel, G.B., de Leeuw, J.W., 1994. Laboratory simulation of natural sulphurization: II. Reaction of multi-functionalized lipids with inorganic polysulphides at low temperatures. Organic Geochemistry 22, 825–834.
- Schubel, J.R., Pritchard, D.W., 1986. Responses of Upper Chesapeake Bay to variations in discharge of the Susquehanna River. Estuaries 9, 236–249.
- Seidel, M., Beck, M., Riedel, T., Waska, H., Suryaputra, I.G.N.A., Schnetger, B., Niggemann, J., Simon, M., Dittmar, T., 2014. Biogeochemistry of dissolved organic matter in an anoxic intertidal creek bank. Geochimica et Cosmochimica Acta 140, 418-434.
- Shakeri Yekta, S., Gonsior, M., Schmitt-Kopplin, P., Svensson, B.H., 2012. Characterization of dissolved organic matter in full scale continuous stirred tank biogas reactors using ultrahigh resolution mass spectrometry: A qualitative overview. Environmental Science & Technology 46, 12711–12719.
- Sharpless, C.M., Blough, N.V., 2014. The importance of charge-transfer interactions in determining chromophoric dissolved organic matter (CDOM) optical and photochemical properties. Environmental Science. Processes & Impacts 16, 654-671
- Shen, C., Testa, J.M., Ni, W., Cai, W., Li, M., Kemp, W.M., 2019. Ecosystem metabolism and carbon balance in Chesapeake Bay: A 30-year analysis using a coupled hydrodynamic-biogeochemical model. Journal of Geophysical Research: Oceans 124, 6141–6153.
- Skoog, A., Hall, P.O.J., Hulth, S., Paxeus, N., Rutgers van der Loeff, M., Westerlund, S., 1996. Early diagenetic production and sediment-water exchange of fluorescent dissolved organic matter in the coastal environment. Geochemistry, Geophysics, Geosystems 60, 3619–3629.
- Spencer, R.G.M., Aiken, G.R., Wickland, K.P., Striegl, R.G., Hernes, P.J., 2008. Seasonal and spatial variability in dissolved organic matter quantity and composition from the Yukon River basin. Alaska. Global Biogeochemical Cycles 22. https://doi.org/ 10.1029/2008GB003231.
- Stenson, A.C., Marshall, A.G., Cooper, W.T., 2003. Exact masses and chemical formulas of individual Suwannee River fulvic acids from ultrahigh resolution electrospray ionization Fourier transform ion cyclotron resonance mass spectrometry. Analytical Chemistry 75, 1275–1284.

- Stirchak, L.T., Moor, K.J., McNeill, K., Donaldson, D.J., 2019. Differences in photochemistry between seawater and freshwater for two natural organic matter samples. Environmental Science: Processes and Impacts 21, 28–39.
- Stubbins, A., Niggemann, J., Dittmar, T., 2012. Photo-lability of deep ocean dissolved black carbon. Biogeosciences 9, 1661–1670.
- Stubbins, A., Lapierre, J.F., Berggren, M., Prairie, Y.T., Dittmar, T., Del Giorgio, P.A., 2014. What's in an EEM? Molecular signatures associated with dissolved organic fluorescence in boreal Canada. Environmental Science and Technology 48, 10598–10606.
- Sturdivant, S.K., Díaz, R.J., Llansó, R., Dauer, D.M., 2014. Relationship between hypoxia and macrobenthic production in Chesapeake Bay. Estuaries and Coasts 37, 1219-1232
- Thang, N.M., Brüchert, V., Formolo, M., Wegener, G., Ginters, L., Jørgensen, B.B., Ferdelman, T.G., 2013. The impact of sediment and carbon fluxes on the biogeochemistry of methane and sulfur in littoral Baltic Sea sediments (Himmerfjärden, Sweden). Estuaries and Coasts 36, 98–115.
- Timko, S.A., Gonsior, M., Cooper, W.J., 2015a. Influence of pH on fluorescent dissolved organic matter photo-degradation. Water Research 85, 266–274.
- Timko, S.A., Maydanov, A., Pittelli, S.L., Conte, M.H., Cooper, W.J., Koch, B.P., Schmitt-Kopplin, P., Gonsior, M., 2015b. Depth-dependent photodegradation of marine dissolved organic matter. Frontiers in Marine Science 2, 1–13.
- Tseng, L.Y., Gonsior, M., Schmitt-Kopplin, P., Cooper, W.J., Pitt, P., Rosso, D., 2013. Molecular characteristics and differences of effluent organic matter from parallel activated sludge and integrated fixed-film activated sludge (IFAS) processes. Environmental Science and Technology 47, 10277–10284.
- Tziotis, D., Hertkorn, N., Schmitt-Kopplin, P., 2011. Kendrick-analogous network visualisation of ion cyclotron resonance Fourier transform mass spectra: improved options for the assignment of elemental compositions and the classification of organic molecular complexity. European Journal of Mass Spectrometry 17, 415–421.
- Vairavamurthy, A., Mopper, K., 1987. Geochemical formation of organosulphur compounds (thiols) by addition of H₂S to sedimentary organic matter. Nature. https://doi.org/10.1038/329623a0.
- Vairavamurthy, A., Zhou, W., Eglinton, T., Manowitz, B., 1994. Sulfonates: A novel class of organic sulfur compounds in marine sediments. Geochimica et Cosmochimica Acta 58, 4681–4687.
- Valle, J., Gonsior, M., Harir, M., Enrich-Prast, A., Schmitt-Kopplin, P., Bastviken, D., Conrad, R., Hertkorn, N., 2018. Extensive processing of sediment pore water dissolved organic matter during anoxic incubation as observed by high-field mass spectrometry (FTICR-MS). Water Research 129, 252–263.
- van Krevelen, D.W., 1950. Graphical-statistical method for the study of structure and reaction processes of coal. Fuel 29, 269–284.
- Viollier, E., Inglett, P.W., Hunter, K., Roychoudhury, A.N., Van Cappellen, P., 2000. The ferrozine method revisited: Fe(II)/Fe(III) determination in natural waters. Applied Geochemistry 15, 785–790.
- Yamashita, Y., Tanoue, E., 2008. Production of bio-refractory fluorescent dissolved organic matter in the ocean interior. Nature Geoscience 1, 579–582.
- Yamashita, Y., Tsukasaki, A., Nishida, T., Tanoue, E., 2007. Vertical and horizontal distribution of fluorescent dissolved organic matter in the Southern Ocean. Marine Chemistry 106, 498–509.
- Zepp, R.G., Sheldon, W.M., Moran, M.A., 2004. Dissolved organic fluorophores in southeastern US coastal waters: correction method for eliminating Rayleigh and Raman scattering peaks in excitation-emission matrices. Marine Chemistry 89, 15–36
- Zhao, Z., Gonsior, M., Luek, J., Timko, S., Ianiri, H., Hertkorn, N., Schmitt-Kopplin, P., Fang, X., Zeng, Q., Jiao, N., Chen, F., 2017. Picocyanobacteria and deep-ocean fluorescent dissolved organic matter share similar optical properties. Nature Communications 8, 1–10.
- Zheng, G., Digiacomo, P.M., Kaushal, S.S., Yuen-Murphy, M.A., Duan, S., 2015. Evolution of sediment plumes in the Chesapeake Bay and implications of climate variability. Environmental Science and Technology 49, 6494–6503.
- Zimmerman, A.R., Canuel, E.A., 2001. Bulk organic matter and lipid biomarker composition of Chesapeake Bay surficial sediments as indicators of environmental processes. Estuarine, Coastal and Shelf Science 53, 319–341.